$2 mi4$

Analysis of Imp-C Data from the Magnetospheric Tail

T. W. Speiser

Principal Investigator

Department of Astro-Geophysics

University of Colorado

Boulder, Colorado 80302

FINAL TECHNICAL REPORT

I.   Introduction

The object of this study was to utilize satellite magnetic field
measurements in the geomagnetic tail current sheet (CS), to try to deter-
mine the normal field component, and other CS parameters such as thickness,
motion, vector current density, etc., and to make correlations with auroral
activity as measured by the A_e index. The satellite data used in the ini-
tial part of this study was from the Imp-C satellite, and later, in an ex-
tention of this grant, data from Imp-4 (Imp-F or Explorer 34) was analyzed.

The geomagnetic tail is formed due to a "frictional interaction"
between the solar wind and the magnetosphere at the boundary, the magneto-
pause. This "frictional interaction" could be due to a classical or non-
classical (instabilities) viscosity, or to magnetic stresses across the
boundary due to field line reconnection along the dayside magnetopause.
It is presently generally agreed that reconnection plays an important --
if not dominant -- role in tail formation.

As magnetic field lines are dragged back into the tail, a region
of reversed magnetic field is created in the center of the tail, since
field lines of opposite polarity are dragged back from the earth's north
and south polar regions. In this region a CS must form for consistency
with Maxwell's equation. The nature of the particles or plasma which con-
tribute to this current has been the object of many observational and
theoretical studies.

If dayside reconnection is the major factor in tail formation,
then magnetic field lines from the dayside magnetosphere are continuously
or sporadically eroded into the tail. In order that the magnetosphere
not disappear after some time, a convection process in the magnetosphere

must be set up to return tail field lines to the dayside magnetosphere. The tail field lines must therefore break, reconnect, and convect toward the earth. Such reconnection will be accompanied by a cross tail electric field which can energize particles in the weak magnetic field CS region, and then further convect plasma toward the earth. When reconnection occurs in the tail, an x-type neutral point or line will be formed in the CS, and it is at this point or line that reconnection occurs. Only at that point or line should the magnetic field be identically zero. Earthward of the reconnection region there will be a weak northward-pointing normal component which gradually increases, eventually matching dipolar values in the near earth equatorial plane. In the opposite direction, the normal component should be weak and southward, eventually merging with the interplanetary magnetic field.

One of the objects of this study is therefore to determine the sign and strength of the CS normal magnetic field component to see if the reconnection region can be within about 40 earth-radii (R_e). We will furthermore investigate correlations of the normal field with A_e as well as with spatial position in the tail and with other CS parameters.

Part II presents the results of the Imp-C (Imp-3) analysis. Forty-eight CS crossings were analyzed from data taken from March-April 1966. Part III presents results from analyzing Imp-F (Imp-4) data, taken from February-May 1968. Part IV summarizes results and conclusions of this study.

II.   Results of the Imp-C Analysis

1.   Data rotations to the frame of the sheet

The characteristics of the tail current sheet, CS, have been measured for 48 CS crossings by the Imp-C satellite. These crossings are summarized in Table 1. During the time of each crossing, linear fits to x, y, z solar-magnetospheric 20-second data points were made. This linearly approximated data was then rotated to the frame of the sheet. The frame of the sheet is defined as that frame where all of the time variation is in one magnetic field component, with the other two components approximately constant during the crossing. The constant components then define the magnetic field component perpendicular to the sheet and thus the orientation of the sheet normal with respect to the solar-magnetospheric system. In order to make such rotations, we assume the sheet is well defined, there are no explicitly time varying fields during the crossing, and there is no variation of the magnetic field with satellite motion parallel to the sheet. Such general rotations of the data can be made whenever the linear approximations are a good fit to the data. The magnitude of the errors incurred because of the invalidity of one or more of the above assumptions can be estimated by making other "extreme" linear approximations to the data. This method is reported in the following as "analysis errors."

Figures 1 through 6 show samples of current sheet crossings. Only three data points from each 5.46 minute interval are shown, although all of the data was used for making the linear approximations which are indicated on the figures. The time scale for each figure can be obtained from Table 1. The left-side of each figure shows the original data and straight line fits in the solar-magnetospheric system, and the right-side

shows the data in the frame of the sheet. The rotations are made as follows: The first rotation is an angle ϕ, about the y_{sm} axis, with $\phi > 0$ meaning the new x' axis is tipped down (southward) and $\phi > 0$ meaning a tipping up with respect to the earth-sun line. The magnitude of ϕ is determined by the variation in B_x and B_z, for constant initial B_z, ϕ is zero. (See Appendix A.) The second rotation is an angle ψ, about the new z' axis, with $\psi < 0$ meaning the projection of the x' axis onto the sm equatorial plane swings toward the dusk side of the earth-sun line, and $\psi < 0$ toward dawn. The magnitude of ψ depends on the variation of B_x and B_y. The magnitude of the normal component, $B_\perp$, is the square root of the sum of the squares of the rotated (constant) y and z components, and is shown in Table 1 for the 48 crossings.

From Table 1, we see that the CS crossings were made at radial distances from 26 to 38 R_e (earth-radii), from 16 R_e near the dawn edge of the tail to 24 R_e near the dusk edge (y_{sm}), and from 6 R_e below to 4 R_e above the solar-magnetospheric equator ($z_{sm} = 0$). The asymmetry of the crossings with y_{sm} is indicative of the aberration angle of the magnetopause due to the earth's heliocentric velocity, and is consistent with the picture presented by Behannon (1970).

The magnitude of $B_\perp$ is shown as a function of radial distance in Figure 7. In Figure 8 we plot the analysis error bars on the determination of $B_\perp$. This error, $\Delta B_\perp$, is one quarter of the difference between maximum and minimum $B_\perp$ values from the linear extremes for each crossing. This evaluation is used to approximate a rms deviation. Figures 9 and 10 are plots of $B_\perp \pm \hat{s} \cdot \hat{n}$, where $\hat{s}$ is the unit vector in the direction of the spin axis of the satellite and $\hat{n}$ is the calculated unit vector normal to the sheet. These plots indicate the error introduced from the larger

uncertainty of the measurements along the spin axis.

From these results we can make the following conclusions for the 48 CS crossings: The average normal component is $+2.9\gamma$ (northward) with a standard deviation of 1.7γ and only three crossings (30, 33, and 46), exhibit weak southward normal components. From Figure 8 we see that the analysis errors may at times be of the order of 1γ, so these "southward" values are not unambiguous. Considering the larger uncertainty of the measurements along the spin axis, from Figure 10 we see that those three values become weaker and one value becomes northward. No additional southward components are introduced due to the uncertainty of the magnetic field component along the spin axis.

The average value of $B_\perp$ for 14 fast crossings (duration of the crossing less than 20 minutes) is 2.2γ. Fast crossings may imply a thinner than average sheet. The weaker values of $B_\perp$ imply a smaller radius of curvature of the field and thus a thinner sheet.

From Figure 8, $\Delta B_\perp$ appears to increase with radial distance, thus the validity of the original assumptions appears to decrease with geocentric distance. From Figure 7 we see no dependence of $B_\perp$ with R, and from Figure 11, there is no apparent dependence of $B_\perp$ with crossing positions projected onto the solar-magnetospheric equatorial plane.

The angles δ, and ρ, are defined as the angles required to rotate z_{sm} into the sheet normal, first about y_{sm} (δ), and secondly about the new x' axis. (See Appendix A.) A summary of the angles, δ, for the 48 crossings is given in Figure 12. The error bars are approximately $\pm 5^{o}$ near dawn, $\pm 20^{o}$ near midnight, and $\pm 10^{o}$ near dusk.

A summary of the current per unit length from curl $\underset{\sim}{B}$ is given in Figure 13. (See Appendix B.) The current density could be determined

for each crossing by dividing by the sheet thickness for that crossing if it were known. Note that the current is generally across the tail from dawn to dusk, with an average component down the tail in the dawn side of the tail. Table 2 gives the averages of the rotation angles δ and ρ, and the current density. For the dawn side of the tail ($y_{sm} < 0$) there is a net current component down the tail (-x direction), but there is no net current in the x-direction for the dusk half of the tail. This current component down the tail on the dawn side agrees with the Imp-A results (Speiser and Ness, 1968), although there was not equivalent coverage by the satellite on the dusk side, so the asymmetry was not observed.

From Table 2, there appears to be a net tipping up of the CS with respect to the earth-sun line for $y_{sm} < -5R_e$, but no other net tippings are apparent. On some individual orbits, tippings of the order of 30° or more are observed. (Note that the standard deviation of all δ's is 24°, and 38° for all ρ's.) Therefore, normal field components made without regard to these inclinations could be in error. As an example, Figure 14 shows the values of the z-component of the field in the solar-magnetospheric system near a neutral sheet crossing. Comparing these results with Figure 7, we see that many more southward components are erroneously determined if we do not consider the orientation of the sheet. Note that the normal component can be determined by measuring the direction and magnitude of the magnetic field at the *exact* time of observation of the minimum in the total magnetic field. This method has the advantage of simplicity, but it has several disadvantages. The first disadvantage is that this method is accurate for only one or two data points *at* the minimum of $|\underset{\sim}{B}|$. (The linear approximation method, however, uses all of the data during a sheet crossing.) Secondly, this cannot distinguish between "anomalous" normal

components at the center of the sheet which may be produced by enhanced filamentary currents within the sheet. Such enhanced filamentary currents may produce either northward or southward perpendicular fields at the center of the sheet. Finally, if data points are taken near the minimum of $|\underset{\sim}{B}|$ but not exactly at this minimum, then a tipping of the sheet with respect to the solar-magnetospheric equatorial plane can result in parallel field components being taken as part of the perpendicular field and vice versa, as shown in Figure 14. Some of the normal components reported by Mihalov, et al. (1968) from Explorer 33 measurements may not be true normal components, since CS orientation was not considered.

2. Rooting distance of the sheet

The simple rooting distance of the CS is defined as $R_o = z_{sm}/\sin \chi_{ss}$, where z_{sm} and χ_{ss} values are given in Table 1. For Imp-A, Speiser and Ness (1968) found that R_o has an average value of 10 R_e with a standard deviation of 3 R_e for measurements near the midnight meridian plane. The average R_o values for Imp-C are given in Table 2. Only cases with $\chi_{ss} > 5^o$ are considered, as positional error of the sheet can give large uncertainties for small χ_{ss}. For these measurements the average R_o is about 14 R_e with a standard deviation of 7 R_e for measurements within 5 R_e of the midnight meridian. The fluctuation is so large that it would be unreasonable to use a given value of R_o to predict the CS position in the absence of magnetic field measurements.

Another parameter is a "circular hinging distance," R_c, as suggested by Russel and Brody (1967). This assumes the CS has a circular shape with the center of the circle on the x_{sm} axis, and the formula is:

$$z' = (R_c^2 - y_{sm}^2)^{1/2} \sin \chi_{ss} \quad .$$

Russel and Brody found their best fit with $R_c = 11\ R_e$, using Imp-A data, with y_{sm} values less than $11\ R_e$. For the Imp-C results, we find the value of R_c for each crossing knowing the crossing position and χ_{ss}. The average value of R_c is $17.5\ R_e$ with a standard deviation of $6\ R_e$ for all the data. From the standard deviation, R_c does not appear to be a better parameter than R_o. However, we will see in the next section that R_c does have a high correlation with the A_e index and R_o does not for these Imp-C measurements.

Note that there is an inherent ambiguity in the use of these types of rooting distance as there may be times when z_{sm} and χ_{ss} have opposite signs. In fact, 18 of the 48 crossings in Table 1 have this characteristic. Taking the meaning of the rooting distance literally would imply, at these times, that the CS is rooted in the day-side magnetosphere! Physically the problem probably arises when the CS is not parallel to the solar-magnetospheric equatorial plane. Thus a positive angle of χ_{ss} should imply the CS being found above the solar-magnetospheric equator, but if the CS is somehow bent down, it may be found below that plane.

Suth bending might be expected to be correlated with magnetospheric dynamics, such as the magnetospheric substorm. Therefore it is worthwhile to see if these rooting parameters, with positive or negative values, have any correlation with ground measurements of magnetic activity. These correlations are made in the next section.

Fairfield and Ness (1970) have suggested an elliptical hinging distance, defined in Table 3, as appropriate. For these measurements we find the average value of R_{16} to be $12 \pm 9\ R_e$ (22 cases) and the average

value of R_{24} to be $7.5 \pm 10 \, R_e$ (31 cases). This parameter does not seem to order the data as well as the circular hinging distance. See also the following section.

In all of these formulas (simple, circular, and elliptical), we note that for χ_{ss} approaching zero, the CS should be found coincident with the sm equator. However, from Table 1, we find that for $\chi_{ss} < 5^o$ (12 cases), the average values of Z_{sm} and $|Z_{sm}|$ are: $<Z_{sm}> = -.58$ and $<|Z_{sm}|> = 2.05$; for $\chi_{ss} < 10^o$ (17 cases), $<Z_{sm}> = -.1$, and $<|Z_{sm}|> = 2.03$. (For Imp-A the corresponding values are: $\chi_{ss} < 5^o$, $<Z_{sm}> = 0.0$, $<|Z_{sm}|> = 0.54$; $\chi_{ss} < 10^o$, $<Z_{sm}> = -.62$, $<|Z_{sm}|> = 0.93$.) Therefore, either some sort of correction must be made to these formulas which is independent of χ_{ss}, or this scatter is due to the flapping motion of the CS. Hruska and Hruskova (1970) suggest the polarity of the radial component of the interplanetary magnetic field plays a role. If so, this should be evidence for the Dunges (open) model of the magnetosphere. Since the above averages of Z_{sm} are small while the averages of $|Z_{sm}|$ are as much as $2 \, R_e$, these results are consistent with a flapping sheet and emphasize the error in assuming that the CS lies in the sm equatorial plane for small χ_{ss}.

3.   Correlations with magnetic activity

Table 3 presents a summary of correlation coefficients, σ, between various parameters used in this study. The "t-test" is a test of the significance of the results, that is, it gives the probablity that a given correlation coefficient could be determined from a set of random numbers. The fifth column gives the observed t-value ($t_{obs} = \sigma\sqrt{N-2}/\sqrt{1-\sigma^2}$, N is the number of cases), the sixth column gives the t-value for 1 percent

probability of chance occurrence. Only t-values for $\sigma > .10$ are given. These correlation coefficients that are significant (whose t-values are larger than the 5 or 1 percent values) are underlined.

The best correlation is item 1, for $|R_c|$ and the A_e index. The corresponding value of σ is $-.70$ with a probability less than .0005 of being produced by a random set of numbers. The correlation of $|R_c|$ with ΣK_p (item 5) is not quite so good ($-.58$), so further correlations were made only with the A_e index.

The best linear fit to the $|R_c|$ and A_e data from a linear regression is

$$|R_c| = -.041 \, A_e + 22.8 \quad .$$

From the spread in the data about the linear fit, we see that if the above formula were used to predict the position of the CS, with known values of A_e, $|R_c|$ would be good to within $\pm 3 \, R_e$, for half the cases, and the absolute value of z_{sm} would be known to about $\pm 1/2 \, R_e$. Unfortunately the determination is double valued. However, we see in Table 1 that if we restrict the range in y_{sm} to crossings with $|y_{sm}| < 10 \, R_e$, than only two cases appear with χ_{ss} and Z_{sm} having opposite signs (crossings 13 and 16). For these crossings, excluding numbers 13 and 16, we find the average value of R_c to be $16 \pm 5 \, R_e$. The correlation coefficient with A_e is $-.71$ (Table 3, item 30) with the probability for chance occurrence still much less than 1 percent. The linear fit is:

$$R_c = -0.36 \, A_e + 21.7 \quad , \qquad |y_{sm}| < 10 \, R_e \qquad ,$$

therefore, this relationship does present the possibility of prediction of the CS z_{sm} position for $|y_{sm}| < 10 \, R_e$ in the tail, knowing χ_{ss}, y_{sm},

and A_e. We cannot say whether or not an x-dependency should be included, that is, whether or not these results hold for crossing distances larger than about 40 R_e.

Because most of the negative rooting distances occur for $|y_{sm}| >$ 10 R_e, a model incorporating this behavior would seem approprriate. Accordingly we tested a model with circular cross section, with the center of the circle translated to negative z_{sm} values for positive χ_{ss}. The model also keeps fixed a chord of length 20 R_e lying in the sm equatorial plane, i.e., the circle always crosses the sm plane at $y_{sm} = \pm$ 10 R_e. This model then eliminates the sign ambiguity for all but 6 of the 48 cases. The average value of R_T (rooting distance of the translated circular cross section) is 13 $\pm$ 12 R_e, and there is no correlation with A_e, item 21, therefore this model, while resolving the sign ambiguity, does not order data very well.

Items 10 and 11 in Table 3 give the correlation between the "elliptical" hinging distance and A_e. No correlation is seen with R_{24}, while a significant correlation is seen with R_{16}, perhaps because the cross section is more nearly circular with R_{16}. The correlation of R_{16} and A_e (item 10) is certainly better than R_c and A_e (item 2) but not as good as R_c and A_e (item 20) for $|y_{sm}| < 10$.

No correlation with A_e is seen for the following: flapping of the CS, item 12; the total tipping of the sheet, the uncertainty in this angle, or the angle of tipping about y_{sm}, items 14, 15 and 23; the distance from the solar-magnetospheric equator, item 16; the normal field component, item 17, or; the simple rooting distance, items 6 through 9.

"Noise" is defined as fluctuations of the magnetic field components with a time scale which is small compared to the duration of the sheet

crossing. We see that there is a slight positive correlation between noise and A_e, item 13, indicating that these fluctuations are enhanced in the CS when A_e is large. There is also an enhancement of the current per unit length as A_e increases, item 18. Since J is a measure of the field strength outside the current sheet (see Appendix B), the field strength outside the current sheet appears to become stronger as A_e increases.

The time duration of Imp-C CS crossings appears to decrease for crossings at larger geocentric distances, item 22, but for the Imp-A crossings, item 24, the correlation is not so high, although it is still negative. The Imp-A crossings were mostly between 14 and 30 R_e, while the Imp-C crossings are from 26 to 38 R_e, so it is possible that this effect becomes important for larger distances. Faster crossings imply either a thinner sheet or a faster moving sheet.

4.   Thicknesses and velocities

In the study of Imp-A current sheet crossings (Speiser and Ness, 1968), CS thickness and velocities were estimated statistically. Those results indicated a CS thickness of about 5,000 km near dawn and 500 km near the midnight meridian. In general, it is not possible to determine thickness or motion of the sheet for a single orbit of the satellite. However, when multiple crossings (flapping) occur, we can determine the sheet thickness and motion by assuming that the flapping motion is sinusoidal. This seems the simplest assumption which can be made. The four parameters of the arbitrary sine wave can then be determined by fitting at four points, knowing the satellite motion. The four

points are chosen as the times when the B_x component turns over, and when B_x goes through zero. As an example, Figure 15 shows an example of multiple crossings from Imp-A (Speiser and Ness, 1968, Figure 6), and times T_1 and T_2 are chosen as turning points, that is, times when the sheet velocity equals the satellite velocity, and times T_3 and T_4 are crossing times. Using these parameters, the motion of the sheet center is determined and plotted in Figure 16 along with the satellite motion and the relative motion $(Z_s - Z_c)$, which should reflect the data of Figure 15. The thickness is then just twice the absolute value of $Z_s - Z_c$ at times T_1 and T_4. From Figure 15 we see that these values are about 800 and 1,000 km. These thicknesses should be, however, corrected by a factor $B_x(F)/B_x(T_1 \text{ or } T_2)$, assuming the field does indeed change linearly across the sheet and that this factor corrects for partial sheet crossings. ($B_x(F)$ is the final value of B_x after leaving the reversal region, i.e., $B_x(F) \simeq 10\gamma$ at 0130 hours in Figure 15.) Making this correction, the thicknesses become 1,460 and 1,480 km at times T_1 and T_2.

This technique has been applied to ten cases from the Imp-C data where multiple crossings occurred. These results are summarized in Table 4. There were a few more flapping cases for which we were unable to find a solution to the sine wave equation. The corrected thickness T_1 and T_2 in Table 4 can be compared, and agreement or lack of agreement between them is one indication of the validity of the model. No apparent correlation with A_e is evident from the data. Times for the data in Table 4 can be found in Table 1.

III. Results of the Imp-4 Analysis

Eighty-five CS crossings were selected from Imp-4 magnetic data in the tail from February to May, 1968. Dr. Donald Fairfield, Goddard Space Flight Center, furnished plots of average data (and some detailed data) in SE and SM polar coordinates from which an initial selection of crossings was made. Dr. Fairfield then supplied a tape of the 2.5 sec data at the crossings in Cartesian SM coordinates.

For the selections, crossings that were primarily relatively sharp and clean were selected. Table 5 summarizes the times, satellite coordinates, and normal magnetic field vectors for each of the 85 crossings.

As discussed in section II, the normal component can be determined in two ways: by making a rotation of the data into the frame of the sheet, or by choosing the magnetic field vector at the exact time of the minimum in the magnitude of the field accompanied by a change in the sign of the tail (x-component) field. The former method seemed useful and adequately accurate for the Imp-C data where a magnetic field vector was determined about once every twenty seconds. This method depended upon being able to make reasonably accurate straight line fits to the component data. However, on inspection of the temporally more sensitive (2.5 sec) Imp-4 data, it became apparent that in many cases a straight line fit was not an adequate approximation to some of the components during a crossing. Figure 17 shows an example of multiple crossings (numbers 35-39, Table 5), where, although the x-component data could be reasonably linearly approximated at the crossings, the y- and z-component data change nonlinearly during the crossings. Therefore, the previous rotation scheme used for the Imp-C data (Appendix A) will not work. We decided to use the latter

method above for determining $B_\perp$. Although the former method utilizes

more data during the crossing, it could generally give a somewhat larger

$B_\perp$ than the latter method if $B_\perp$ decreases somewhat during a crossing. Such

a decrease is not expected to be large, but it might be expected from

consideration of a simple tail model where $|B_x|$ decreases with $-x$, and

$\nabla \cdot B = 0$ is required. On the other hand, the minimum B method is more

subject to variations due to spatial irregularities in the current density.

In fact, it was suggested (Speiser, 1973) that the magnetic field signa-

ture of Figure 17 represents a filamentary current structure within the CS.

Correlations of various CS parameters were made with each other in

Table 6. For the correlations, 64 of the 85 crossings were included.

Eleven crossings were eliminated using the criterion that we should have

at most three crossings per hour. The reason for this choice is that many

of the multiple crossings in a short time would tend to bias any correla-

tion to that particular satellite location, or temporally to that particu-

lar state of geomagnetic/tail activity.

For the correlations in this section, the t-test yields the follow-

ing significance criteria (correlation coefficient; probability percent):

(0.40; 0.1 percent), (0.32; 1 percent), (0.25; 5 percent). That is, a

correlation coefficient of 0.32 would be achieved by correlating two ran-

dom sets of 64 numbers only 1 percent of the time, etc.

In Table 6, there are some high correlations of parameters which

should obviously be well correlated. For example, P_x and R_x highly corre-

late with T_x as they should since $T_x = P_x + F_x$, and $|B_\perp|$ correlates highly

with $B_\perp$, $B_{\perp z}$, and B1. Other correlation coefficients of possible signifi-

cance with $|B_\perp|$ are F_x and Y_{sm}. The former implies that $|B_\perp|$ is likely to

be large if there are a large number of complete-multiple crossings, and

the latter that $|B_\perp|$ has a tendency to be larger near the dusk edge of the tail than near the dawn edge. This would tend to support the theoretical prediction of Cowley (1971) for a tail reconnection model.

Some other correlations of interest are: multiple crossings are more likely to occur near the earth (within the range of Imp-4) -- (T_x, R), (T_x, X_{sm}); B3/Δt is proportional to the current density times the relative (sheet-satellite) velocity (jV), if jV is large, noise is large; negative $B_{\perp z}$ is more likely when jV is large; $B_\perp$ is likely to be smallest when jV is large, and; when jV is large, $|Z_{sm}|$ is likely to be small.

The correlations of tail parameters with each other in Table 6 are for all types of geomagnetic activity. The various parameters were therefore correlated with the 2.5 minute A_e index to get an indication of variability with geomagnetic activity. (Note these correlations were done with the A_e index derived from five stations -- the eleven station index was unavailable at the time. A re-calculation using the eleven stations index is being pursued.) These correlations are plotted in Figures 18 and 19. The correlations were done with A_e values at the time of the crossing (0 - abscissa) and for A_e values up to 4 hours before and after each crossing. In Figure 18 we see that B3 (proportional to the current density times the thickness of the CS, or to the current per unit length down the tail) has its maximum positive correlation with A_e about 5 minutes earlier. Therefore, the current/length appears to be largest about 5 minutes after the peak substorm intensity. Many multiple crossings (T_x) are most likely to occur about 30 minutes to 1 hour before the substorm maximum. This probably means "flapping" is induced near the onset of a substorm. The magnitude of the normal component, $|B_\perp|$, seems to be largest about 2 hours before the substorm peak. This would imply the field lines are more

dipolar between substorms, and more stretched out during a substorm. (The $|B_\perp|$ curve does go negative near $t = 0$, but the correlation coefficients are not significant.)

From Figure 19, magnetic noise appears to be largest about 30 minutes after the substorm peak, while the CS tilt angles are largest when a substorm is going on near the time of a CS crossing, and B3/ΔT peaks with A_e values near $t = 0$, in a similar fashion to B3 (Figure 18) but with a smaller correlation.

IV.   Discussion

There is little indication from either Imp-3 or Imp-4 CS crossings of detection of southward normal components, regardless of substorm phase, closer than about 40 R_e in the tail. Certainly some "nonlinear" southward normal components are found probably with enhanced filamentary current systems within the CS -- and that may or may not be the expected signature of a reconnection neutral point or line in the tail. There have recently been some observations that long-lasting southward normal components are found in the near earth tail plasma sheet -- outside of the CS. (See, for example, Nishida and Nagayama, 1973.) If the reconnection is indeed closer to the earth than the satellite near the onset of a substorm, why then do we not see relatively constant southward components at these times? One possibility is that the normal component away from the CS may be influenced by tilting, and therefore not necessarily indicative of the magnetic field through the CS. Another possibility is that the CS normal component is dominated by spatial and temporal irregularities (filamentary

currents, etc.) so that the normal component determined in the external region is more indicative of the real normal component. This question is presently being studied further.

The current density in the CS appears to peak near the peak of a substorm, and the largest tilt angles with respect to Z_{sm} seem to occur at this time, while "flapping" seems to precede substorms, or perhaps occur near a substorm onset, or in the expansion phase.

Further study of questions raised in this study, correlations with particular substorm phase, etc., are being pursued under NASA Grant NGR-06-003-215. A summary publication with the results of this latter study is being prepared.

ACKNOWLEDGEMENTS

Papers Presented (NGR-06-003-092)

"Imp-3 Magnetic Field Measurements within and near the Neutral Sheet," With N. F. Ness, Am. Geophys. Un. meeting, April 1968. Abstract, Trans. Am. Geophys. Un. 49 (1), 281, March 1968.

"Tail Neutral Sheet Orientation and Perpendicular Magnetic Field from the Imp-C Magnetometer Data," with N. F. Ness, Am. Geophys. Un. meeting, April 1969. Abstract, Trans. Am. Geophys. Un. 50 (4), 296, April 1969.

"Evidence for Reconnection at the Day-Side Magnetopause from the ATS-1 Results," Am. Geophys. Un. meeting, April 1969. Abstract, ibid.

"The Flapping Current Sheet in the Geomagnetic Tail," with N. F. Ness, Am. Geophys. Un. meeting, April 1970. Abstract, Trans. Am. Geophys. Un. 51 (4), 403, April 1970.

"Summary of Imp-1 and Imp-3 Magnetic Observations in the Magnetotail," Quantitative Magnetospheric Models meeting, March 1970, Boulder, Colo.

"The Tail Current Sheet from Imp-4 Magnetic Field Data," Am. Geophys. Un. meeting, April 1971. Abstract, Trans. Am. Geophys. Un. 52 (4), 326, April 1971.

"Tail Current Sheet Parameters from Imp-F and Correlations with Auroral Activity," Am. Geophys. Un. meeting, April 1973. Abstract, Trans. Am. Geophys. Un. 54 (4), 426, April 1973.

"Correlations of Tail Current Sheet Parameters and A_e," short paper presented at Magnetospheric-Ionospheric Coupling Symposium, Yosemite, California, February 1974.

Papers Published

Acknowledging support of NGR-06-003-092

"Conductivity without Collisions or Noise," Planet Space Sci. 18, 613-622, 1970.

"The Dungey Model of the Magnetosphere, and Astro-geophysical Current Sheets," Radio Science 6 (2), 315-319, Feb. 1971.

"Mathematical Models of the Open Magnetosphere: Application to Dayside Auroras," with T. G. Forbes, J. Geophys. Res. 76 (31), 7542-7551, Nov. 1971.

"Magnetospheric Plasma: Sources, Wave-Particle Interactions, and Acceleration Mechanisms," J. of Sci. and Ind. Res. 30 (8), 408-413, 1971.

"Magnetospheric Current Sheets," Radio Science 8 (11), 973-977, Nov. 1973.

"Energy and Pitch Angle Distributions for Auroral Ions Using the Current Sheet Acceleration Model," with E. F. Jaeger, Astrophys. and Space Sci., 1974, to be published.

REFERENCES

Behannon, K. W., "Geometry of the Geomagnetic Tail," J. Geophys. Res. 75, 743-753 (1970).

Cowley, S. W. H., "The adiabatic flow model of a neutral sheet," Cosmic Electrodyn. 2, 90-104 (1971).

Fairfield, D. H. and N. F. Ness, "Configuration of the Geomagnetic Tail During Substorms," J. Geophys. Res. 75 (34), 7032 (1970).

Hruska, A. and J. Kruskova, "Transverse structure of the earth's magneto-tail and fluctuations of the tail magnetic field," J. Geophys. Res. 75, 2449-2457 (1970).

Mihalov, J. D., D. S. Colburn, R. G. Currie, and C. P. Sonett, "Configuration and Reconnection of the Geomagnetic Tail," J. Geophys. Res. 73, 943-949 (1968).

Nishida, A. and N. Nugayama, "Synoptic Survey for the Neutral Line in the Magnetotail during the Sbustorm Expansion Phase," J. Geophys. Res. 78 (19), 3782-3798 (1973).

Russell, C. T. and K. I. Brody, "Some Remarks on the Position of the Neutral Sheet," J. Geophys. Res. 72, 6104-6106 (1967).

Speiser, T. W. and N. F. Ness, "The neutral sheet in the geomagnetic tail: Its motion, equivalent currents, and field line reconnection through it," J. Geophys. Res. 72, 131-141 (1967).

Speiser, T. W., "Magnetospheric Current Sheets," Radio Science 8 (11), 973-977, Nov. (1973).

APPENDIX A

Data Rotations

1. Approximate CS data by a linear fit: $B_z = at + b$; $B_y = ct + d$;

   $B_x = et + f$, where t is time, B_x, B_y, B_z, in sm coordinates.

2. Make two rotations to $\underset{\sim}{B}''$; $B_y'' = $ constant, and $B_z'' = $ constant:

$$\underset{\sim}{B}'' = \underset{\sim}{\Psi} \underset{\sim}{\Phi} \underset{\sim}{B}$$

   where

$$\underset{\sim}{\Phi} = \begin{pmatrix} \cos\phi & 0 & -\sin\phi \\ 0 & 1 & 0 \\ \sin\phi & 0 & \cos\phi \end{pmatrix}, \quad \underset{\sim}{\Psi} = \begin{pmatrix} \cos\psi & \sin\psi & 0 \\ -\sin\psi & \cos\psi & 0 \\ 0 & 0 & 1 \end{pmatrix}$$

3. Solutions:

$$\tan\phi = -a/e \quad ; \quad \tan\psi = \pm\, c/a_1$$

$$a_1 = (a^2 + e^2)^{1/2}$$

$$a_2 = (a^2 + c^2 + e^2)^{1/2}$$

$$a_3 = ab + cd + ef$$

$$a_4 = ab + ef$$

$$a_5 = be - af$$

$$B_x'' = \pm\, (a_2 t + a_3/a_2)$$

$$B_y'' = [da_1^2 - ca_4]/a_1 a_2$$

$$B_z'' = \pm\, a_5/a_1$$

$$B_\perp = (B_z''^2 + B_y''^2)^{1/2} \times (\text{sign of } B_z'')$$

   where $\pm$ sign chosen to make slope of B_x'' in the same direction as

   the slope of B_x.

4. Rotate $\underset{\sim}{B}_\perp$ back to sm system to get $B_{x\perp}$, $B_{y\perp}$, $B_{z\perp}$. Then: $\tan\delta = B_{x\perp}/B_{z\perp}$; $\tan\rho = B_{y\perp}/(B_{x\perp}^2 + B_{z\perp}^2)^{1/2}$.

APPENDIX B

Evaluation of the Current per Unit Length, $\underset{\sim}{J}$

$$\frac{\mu_o \underset{\sim}{J}}{T} = \mu_o \underset{\sim}{j} = \underset{\sim}{\nabla} \times \underset{\sim}{B} \approx \frac{\Delta B_y}{\Delta z} \hat{e}_x + \frac{\Delta B_x}{\Delta z} \hat{e}_y$$

where the latter values are taken in the "prime" system, after the first rotation, ϕ. (Appendix A.)

Then:

$$J_x = -\Delta B_y \cdot (\text{sign of } \Delta B_x) / \mu_o$$

$$J_y = |\Delta B_x| / \mu_o$$

assuming $T \approx \Delta z$.

Table 1

IMP-C NEUTRAL SHEET CROSSINGS, 1966

(48 Crossings)

Orbit	Cross-ing Number	Length of Crossing- (in Min)	day	Time of Crossing hour	min.	Position of Satellite (in Re)				Perpendicular Magnetic Field of Crossing $B_\perp$	γ_s
						X(SM)	Y(SM)	Z(SM)	R		
48	1	43.68	63	7	24.3	-21.9521	-16.5147	.0753	27.4707	5.48	-15.59
48	2	180.18	63	8	10.1	-21.5110	-16.3473	.8175	27.0301	3.49	-13.80
49	3	32.76	68	11	51.7	-30.7682	-15.3759	-3.5152	34.5754	3.04	- 1.30
49	4	92.82	68	13	26.4	-30.2566	-15.2222	-3.5539	34.0559	4.32	2.33
49	5	76.44	68	14	17,6	-29,9525	-15,0982	-3.7625	33.7530	5.10	4.88
49	6	38.22	69	3	55.8	-23,6521	-14.3843	-1.2209	27.7095	4.09	-15.70
49	7	98.28	69	5	38.3	-22,5798	-14.2478	.8143	26.7116	4.51	-15.70
50	8	49.14	75	2	38.2	-22.4039	-12.1378	.4438	25.4844	3.19	-11.94
51	9	38.22	80	22	10.4	-23.3601	-10.2538	.8052	25.5241	1.49	2.00
52	10	16.38	85	22	57.2	-33.6436	- 5.1765	-2.8781	34.1610	3.83	1.59
52	11	16.38	86	0	26.9	-33.1333	- 5.5394	-2.3580	33.6758	4.97	-2.77
52	12	16.38	86	3	18.5	-32.0182	- 6.3467	-.8328	32.6335	2.40	-8.57
52	13	16.38	86	6	4.2	-30.8194	- 6.6054	.9656	31.5343	1.57	-8.49
52	14	38.22	86	15	6.6	-25.8168	- 7.3494	3.8860	27.1224	2.15	13.24
52	15	38.22	86	16	45.7	-24.6723	- 7.8067	3.7116	26.1427	3.00	14.31
53	16	21.84	91	20	39.7	-33.0494	- 3.1534	-.1131	33.1997	4.80	10.36
53	17	32.76	92	1	10.1	-31.1693	- 4.1458	1.1520	31.4649	5.54	-2.47
53	18	5.46	92	1	44.8	-30.9020	- 4.2450	1.3961	31.2231	2.28	-3.78
53	19	5.46	92	1	45.9	-30.9020	- 4.2450	1.3961	31.2231	3.16	-3.78
54	20	81.90	97	4	34.5	-36.5492	1.9460	-1.2404	36.6219	3.34	-5.05
54	21	60.06	97	5	30.4	-36.3864	1.7156	-1.0533	36.4421	5.17	-4.74
54	22	32.76	97	20	37.9	-31.6771	- 2.0543	3.1317	31.8977	1.74	12.53
54	23	27.30	97	20	42.2	-31.6771	- 2.0542	3.1317	31.8977	.97	12.53
54	24	92.82	97	22	19.0	-30.9104	- 2.5720	3.4547	31.2090	2.66	7.70
54	25	65.52	97	22	26.4	-30.8715	- 2.5967	3.4760	31.1749	2.24	7.45
55	26	49.14	103	7	48.6	-34.7498	4.1299	1.4860	35.0259	3.07	1.07
55	27	21.84	103	8	36.8	-34.5430	4.0255	1.6220	34.8146	4.28	2.90
55	28	21.84	103	8	45.0	-34.4979	4.0011	1.6659	34.7691	2.86	3.34

Orbit	Crossing Number	Length of Crossing- (in Min)	day	Time of Crossing hour	min.	Position	of	Satellite	(in Re)	Perpendicular Magnetic Field of Crossing $B_\perp$	χ_{ss}
						X(SM)	Y(SM)	Z(SM)	R		
55	29	21.84	103	11	45.3	-33.5826	3.4997	2.5586	33.8613	6.23	12.23
55	30	10.92	103	11	51.7	-33.5573	3.4748	2.5949	33.8364	-.41	12.47
55	31	10.92	103	12	5.7	-33.4737	3.4213	2.6796	33.7546	2.53	13.20
55	32	10.92	103	12	15.3	-33.4195	3.3774	2.7516	33.7022	4.38	13.67
55	33	10.92	103	12	28.5	-33.3344	3.3205	2.8493	33.6203	-1.13	14.37
55	34	16.38	103	12	47.6	-33.2436	3.2472	2.9506	33.5319	1.96	15.04
56	35	21.84	108	21	58.4	-35.5354	8.1437	3.2868	36.6044	2.77	12.47
56	36	10.92	108	22	25.7	-35.4747	8.0206	3.3891	36.5276	.72	11.21
56	37	21.84	108	22	35.1	-35.4509	7.9757	3.4272	36.4983	.45	10.70
58	38	38.22	119	20	4.6	-33.1518	18.7175	1.2037	38.0899	1.49	-21.33
59	39	21.84	125	16	5.1	-31.3256	21.1865	-1.9723	37.8689	2.86	27.86
59	40	16.38	125	16	38.8	-31.3943	21.1766	-1.0507	37.8834	2.35	27.95
59	41	16.38	125	17	0.3	-31.4266	21.1594	- .5390	37.8898	2.44	27.87
59	42	21.84	125	17	23.9	-31.4688	21.1077	.1122	37.8923	1.69	27.64
59	43	49.14	125	17	39.5	-31.4943	21.6668	.4848	37.8938	2.70	27.43
59	44	87.36	126	10	54.5	-31.4040	18.3434	.4154	36.3713	1.73	17.26
60	45	21.84	131	11	12.2	-29.0341	23.3691	-6.5758	37.8462	6.37	19.36
60	46	38.22	131	11	32.5	-29.0865	23.3821	-6.3645	37.8583	-.72	20.61
60	47	27.30	131	14	27.5	-29.4095	23.6870	-3.2333	37.9005	2.58	27.81
60	48	21.84	131	14	54.4	-29.4391	23.7195	-2.5865	37.8941	2.83	28.45

Table 2

Averages of δ and ρ ($\pm \sigma$)

All Y_{sm} ; $\bar{\delta} = -8 \pm 24$; $\bar{\rho} = 6 \pm 38$

$Y_{sm} < -5$; $\bar{\delta} = -21 \pm 11$; $\bar{\rho} = 15 \pm 24$

$-5 < Y_{sm} < 5$; $\bar{\delta} = -6 \pm 28$; $\bar{\rho} = 8 \pm 38$

$Y_{sm} > 5$; $\bar{\delta} = 1 \pm 22$; $\bar{\rho} = -5 \pm 40$

Orbit 48 ; $\bar{\delta} = -42 \pm 5.3$; $\bar{\rho} = +11.1 \pm 0$

Orbit 49 ; $\bar{\delta} = -19 \pm 6$; $\bar{\rho} = -10 \pm 5$

Averages of Current Components ($\pm \sigma$)

All Y_{sm} ; $\bar{J}_x = -.19 \pm .30$; $\bar{J}_y = 1.27 \pm .55$

$Y_{sm} < 0$; $\bar{J}_x = -.35 \pm .15$

$Y_{sm} > 0$; $\bar{J}_x = -.08 \pm .32$

Averages of R_o ($\chi_{ss} > 5^o$) ($\pm \sigma$)

All R_o ; $\bar{R}_o = 5.3 \pm 10.9$

$-5 < Y < 5$; $\bar{R}_o = 13.7 \pm 6.6$

Orbit 60 ; $\bar{R}_o = -12.6 \pm 6.4$

Table 3

Correlation Coefficients

Item	Parameters	No. of Cases	α	$t_{obs.}$	t(.05)	t(.01)
1.	$|R_c|$ vs. A_e	35	-.70	5.5	2.04	2.75
2.	R_c vs. A_e	35	+.19	1.14	2.04	2.75
3.	R_c^+ vs. A_e	21	-.69	4.37	2.09	2.86
4.	R_c^- vs. A_e	14	+.72	3.88	2.18	3.06
5.	$|R_c|$ vs. K_p	35	-.58	4.09	2.04	2.75
6.	$|R_o|$ vs. A_e	35	-.02			
7.	R_o vs. A_e	35	+.05			
8.	R_o^+ vs. A_e	21	-.03			
9.	R_o^- vs. A_e	14	+.28	1.09	2.18	3.06
10.	R_{16} vs. A_e	22	-.49	3.22	2.09	2.85
11.	R_{24} vs. A_e	31	-.06			
12.	Flapping vs. A_e	48	+.16	1.09	2.01	2.69
13.	Noise vs. A_e	48	+.31	2.21	2.01	2.69
14.	χ vs. A_e	48	+.09			
15.	$\Delta\chi$ vs. A_e	48	+.15	1.03	2.01	2.69
16.	$|Z_{sm}|$ vs. A_e	48	-.19	1.31	2.01	2.69

Table 3 (Continued)

Item	Parameters	No. of Cases	σ	$t_{obs.}$	t(.05)	t(.01)
17.	B_1 vs. A_e	48	-.03			
18.	$|J|$ vs. A_e	48	+.33	2.37	2.01	2.69
19.	$|Z_c|$ vs. A_e					
20.	R_c vs. A_e, $|Y_{sm}| < 10$	17	-.71	3.90	2.13	2.95
21.	R_t vs. A_e	29	+.01			
22.	Δt vs. R (Imp-c)	48	-.30	2.13	2.01	2.69
23.	δ vs. χ_{ss}	48	+.20	1.38	2.01	2.69
24.	Δt vs. R (Imp-a)	34	-.20	1.18	2.04	2.75

Parameters

σ — Correlation coefficient

A_e — Auroral electrojet index, hourly values.

K_p — Magnetic activity, (ΣK_p), 3 hour index.

R_c — Circular hinging distance, after Russel and Brody, see text.

R_c^+ — Circular hinging distance, positive values only

R_c^- — Circular hinging distance, negative values only

$|R_c|$ — Circular hinging distance, absolute value

R_o — Rooting distance; $R_o = Z_{sm} / \sin \chi_{ss}$

R_{16} — Elliptical hinging distance; $R_{16} = Z_{sm}/ \left[(1-(Y_{sm}/16)^2)^{\frac{1}{2}}\sin \chi_{ss}\right]$ for $|Y_{sm}| < 16\ R_e$

R_{24} — Elliptical hinging distance; $R_{24} = Z_{sm}/ \left[(1-(Y_{sm}/24)^2)^{\frac{1}{2}}\sin \chi_{ss}\right]$ for $|Y_{sm}| < 24\ R_e$

R_t — Translated circle hinging distance, see text.

Flapping — Number of CS crossings near a given crossing

Noise — Fluctuations in magnetic field near a crossing, see text.

χ — The angle between Z_{sm} and the sheet normal

Δχ — Uncertainty in χ from the "analysis errors"

Z_{sm}, Y_{sm} — Solar magnetospheric co-ordinates of satellite position at CS crossing

Table 3 (Continued)

χ_{ss} —   Geomagnetic latitude of the sub-solar point

$B_{\perp}$ —   The normal field component

$|Z_c|$ —   The distance from the average Russel and Brody CS position,

$$|Z_c| = |Z_{sm} - Z|; \quad Z = (17.5^2 - Y_{sm}^2)^{\frac{1}{2}} \sin \chi_{ss}$$

Δt —   The time duration of each crossing

δ —   The first rotation angle, see text

R(Imp-c)-   The radial distance of the Imp-c CS crossings

R(Imp-a)-   The radial distance of the Imp-a CS Crossings

TABLE 4

Thicknesses of Current Sheet, Flapping Model, Imp-C

Imp-C Orbit	Cross'g Number		Satellite x(R_e)	Position y(R_e)	(sm) z(R_e)	Flapp'g Period (min.)	Model Ampl. (km)	THICKNESS		
								T_1(km)	T_2(km)	A_e Hr. av.
49	3		-30.8	-15.4	-3.5	37.9	419	5000	3522	24
49	6		-23.7	-14.4	-1.2	29.4	3088	23400	23072	27
52	13		-30.8	-6.6	.97	37.1	2858	5000	6262	304
55	28	1	-34.5	4.0	1.67	27.6	53.1	301	178	101
55	28	2	-34.5	4.0	1.67	54.2	200	356	657	101
55	30	2	-33.6	3.5	2.59	27.2	940	6160	1290	332
55	33		-33.3	3.3	2.8	24.6	1411	4710	4010	224
59	40		-31.4	21.2	-1.1	34.9	3657	5390	8426	75
60	47		-29.4	23.7	-3.2	66.1	2814	18800	7900	52
60	48		-29.4	23.7	-2.6	74.4	1382	1490	750	52

TABLE 5

-31-

IMP-4 Current Sheet Crossings, 1968

Cross-ing #	Orbit	Date	Crossing Time (hr;min;sec;)	Magnetic field (γ) at crossing (SM)				Xss (x10)	Satellite Co-ordinates (SM)(Re)			
				Bmin	Bx	By	Bz		R	X	Y	Z
1	63	2-18	06; 07; 50	5.7	-1.2	1.9	5.2	-230	30.3	-28.4	-8.1	-6.9
2	63	2-18	06; 18; 15	1.7	-1.4	.1	.9	-228	30.4	-28.5	-8.2	-6.8
3	64	2-19	05; 48; 12	.5	- .1	0.0	.5	-230	33.4	-31.9	-9.7	-2.0
4	64	2-23	07; 21; 50	.6	- .4	-.2	.4	-193	33.5	-32.6	-7.3	-2.2
5	64	2-23	07; 27; 00	.6	.2	-.6	0.0	-192	33.5	-32.6	-7.3	-2.2
6	64	2-23	07; 33; 20	1.1	0.0	.9	.7	-189	33.5	-32.6	-7.3	-2.1
7	64	2-23	09; 02; 50	1.8	.6	-.3	1.7	-152	33.6	-32.7	-7.4	-1.4
8	64	2-23	09; 12; 00	2.6	.7	1.0	2.6	-148	33.6	-32.7	-7.4	-1.3
9	64	2-23	09; 43; 45	.5	- .2	0.0	.5	-132	33.5	-32.7	-7.4	-1.1
10	64	2-23	21; 54; 40	.8	.2	.2	.7	- 69	32.2	-31.4	-7.2	-1.2
11	64	2-24	00; 33; 18	1.6	- .1	-.2	1.6	-148	31.6	-30.7	-7.3	- .5
12	64	2-24	00; 36; 54	.6	- .2	-.2	.5	-150	31.6	-30.7	-7.3	- .5
13	65	2-27	05; 34; 54	.5	- .1	-.1	-.5	-202	32.4	-31.9	-4.2	-4.2
14	65	2-27	05; 35; 42	.3	- .2	-.1	-.2	-202	32.4	-31.9	-4.2	-4.2
15	65	2-27	07; 51; 00	.3	0.0	.3	-.1	-168	32.8	-32.3	-4.7	-3.2
16	65	2-27	08; 15; 48	.6	.1	.4	-.4	-158	32.9	-32.4	-4.8	-3.0
17	65	2-27	08; 37; 00	1.0	.9	0.0	.4	-149	33.0	-32.5	-4.8	-2.9
18	65	2-27	10; 00; 48	.2	- .2	.1	-.2	-108	33.2	-32.7	-4.9	-2.4
19	65	2-27	10; 15; 12	.3	0.0	.3	-.1	-101	33.2	-32.7	-4.9	-2.4
20	65	2-27	19; 28; 48	3.0	2.9	.7	.5	6	33.5	-33.1	-4.6	-1.8
21	65	2-28	02; 29; 30	1.5	-1.4	.4	-.2	-179	32.8	-32.4	-5.1	- .2
22	65	2-28	02; 31; 00	1.8	- .8	1.3	-.9	-180	32.8	-32.4	-5.1	- .2
23	65	2-28	02; 34; 24	2.7	1.8	2.1	-.2	-180	32.8	-32.4	-5.1	- .2
24	66	3-2	01; 20; 12	2.2	0.0	-.6	2.1	-144	28.8	-28.2	.1	-5.9
25	66	3-2	01; 41; 06	3.8	.9	-2.0	3.1	-152	29.0	-28.4	0.0	-5.8
26	70	3-20	15; 07; 20	.9	.8	.3	.2	108	33.2	-32.2	6.6	4.5
27	70	3-20	15; 18; 00	2.8	1.6	1.9	2.1	110	33.2	-32.2	6.6	4.6
28	71	3-23	18; 02; 42	2.6	- .5	1.4	2.1	123	29.4	-28.0	9.1	- .2
29	71	3-23	18; 07; 12	2.7	- .5	1.6	2.1	122	29.4	-28.0	9.1	- .2
30	71	3-23	18; 09; 48	2.4	.4	2.0	1.3	122	29.4	-28.0	9.1	- .2
31	71	3-23	18; 12; 18	2.4	.8	.8	2.1	121	29.6	-28.0	9.5	- .2
32	72	3-27	21; 34; 48	.2	.2	.1	-.1	62	27.5	-25.4	10.5	.9
33	72	3-27	21; 43; 00	.2	.1	.2	0.0	58	27.5	-25.4	10.5	1.0
34	72	3-28	06; 22; 24	.5	- .2	-.2	.4	- 76	30.9	-28.8	11.3	.1
35	72	3-28	11; 19; 42	3.9	.2	-3.7	-1.2	50	32.2	-30.0	11.6	0.0
36	72	3-28	11; 21; 54	4.3	-3.6	.9	2.2	52	32.2	-30.0	11.6	.1
37	72	3-28	11; 25; 36	3.9	2.1	-1.1	-3.1	54	32.2	-30.0	11.6	.1
38	72	3-28	11; 30; 48	4.4	-2.6	-2.7	2.3	56	32.2	-30.0	11.6	.1
39	72	3-28	11; 35; 24	4.3	1.3	.2	-4.1	58	32.2	-30.1	11.6	.1
40	72	3-28	16; 14; 24	.2	.1	-.2	.1	149	33.0	-30.8	11.5	3.4
41	72	3-28	17; 21; 42	.8	- .3	.3	.7	148	33.1	-30.9	11.2	4.3
42	72	3-28	17; 30; 12	.8	.2	-.2	.8	147	33.2	-30.9	11.2	4.5
43	72	3-28	18; 21; 30	.8	.1	-.8	.1	139	33.3	-31.0	10.9	5.2
44	73	3-31	22; 08; 42	4.3	- .8	1.5	4.0	60	23.2	-20.4	11.0	- .2
45	73	3-31	22; 11; 30	5.0	-3.5	-.4	3.5	58	23.2	-20.4	11.0	- .1
46	73	3-31	22; 14; 42	4.3	2.1	2.6	-2.7	57	23.2	-20.4	11.0	- .1

TABLE 5 — Continued   -32-

IMP-4 Current Sheet Crossings, 1968

Cross-ing #	Orbit	Date	Crossing Time (hr;min;sec;)	Magnetic field (𝛾) at crossing (SM) Bmin	Bx	By	Bz	Xss (x10)	Satellite Co-ordinates (SM)(Re) R	X	Y	Z
47	73	3-31	22; 18; 54	3.4	3.3	.2	- .7	55	23.3	-20.5	11.0	- .1
48	73	3-31	22; 19; 48	2.1	.5	.4	2.0	54	23.3	-20.5	11.0	- .1
49	73	3-31	22; 22; 36	1.7	- .1	-1.6	.7	53	23.3	-20.5	11.0	- .1
50	73	3-31	22; 24; 06	1.3	- .4	.3	1.2	52	23.3	-20.5	11.0	- .1
51	73	3-31	22; 27; 30	1.6	- .5	- .4	1.5	50	23.4	-20.6	11.0	- .1
52	73	3-31	22; 34; 06	.9	- .1	.3	.8	47	23.4	-20.6	11.0	0.0
53	73	3-31	22; 37; 12	4.2	-1.5	.9	-3.9	45	23.5	-20.7	11.1	0.0
54	73	3-31	22; 37; 54	7.5	.6	6.0	4.5	45	23.5	-20.7	11.1	0.0
55	73	3-31	22; 39; 30	3.9	-2.7	2.0	-2.0	44	23.5	-20.7	11.1	0.0
56	73	3-31	22; 41; 06	3.3	.8	3.0	-1.2	43	23.5	-20.7	11.0	0.0
57	73	3-31	22; 41; 18	3.4	.3	1.9	-2.8	43	23.5	-20.7	11.1	0.0
58	73	3-31	22; 44; 06	1.2	.4	- .8	- .8	41	23.6	-20.8	11.1	0.0
59	73	4-1	18; 01; 06	1.4	.5	- .5	-1.2	158	31.9	-28.8	13.1	3.9
60	73	4-1	18; 06; 00	2.1	-1.5	.6	1.3	157	31.9	-28.8	13.1	4.0
61	73	4-1	18; 09; 48	.8	.5	.1	.6	157	31.9	-28.8	13.1	4.1
62	74	4-5	13; 49; 18	3.0	.4	1.2	2.7	149	27.6	-23.9	13.9	-1.6
63	74	4-5	13; 52; 54	2.7	.4	.6	2.6	149	27.6	-23.9	13.9	-1.6
64	74	4-5	13; 56; 42	3.0	-1.1	0.0	2.8	151	27.6	-23.9	13.9	-1.6
65	74	4-5	15; 10; 24	1.5	.9	.8	- .9	171	28.2	-24.4	14.2	- .4
66	74	4-5	15; 11; 12	1.4	-1.3	.4	0.0	172	28.2	-24.4	14.2	- .4
67	74	4-5	15; 21; 18	.5	.4	0.0	- .2	174	28.3	-24.5	14.3	- .2
68	74	4-5	15; 30; 00	3.7	-1.6	-1.1	2.9	175	28.5	-24.6	14.3	- .1
69	74	4-5	15; 37; 12	2.7	2.0	1.3	1.3	176	28.5	-24.6	14.3	0.0
70	74	4-5	15; 40; 54	.5	- .1	- .1	- .5	177	28.5	-24.6	14.3	.1
71	74	4-6	00; 09; 00	2.4	-1.4	1.5	1.2	18	31.5	-27.3	14.4	6.1
72	74	4-6	00; 13; 30	1.7	.7	1.4	.7	16	31.5	-27.3	14.4	6.0
73	74	4-6	00; 14; 00	1.9	.3	1.9	.2	16	31.5	-27.3	14.4	6.0
74	76	4-13	21; 23; 24	1.6	- .1	-1.5	.4	128	22.3	-17.1	14.2	1.7
75	76	4-13	21; 24; 06	.8	.6	.1	.6	127	22.3	-17.1	14.2	1.7
76	76	4-13	21; 26; 42	.8	.1	- .8	0.0	126	22.3	-17.1	14.2	1.7
77	76	4-13	21; 29; 54	3.8	2.3	2.6	.1	125	22.3	-17.1	14.2	1.8
78	76	4-14	12; 39; 18	2.4	- .1	- .7	2.3	154	30.2	-23.7	18.7	.1
79	76	4-14	13; 41; 18	5.0	.2	.7	4.9	179	30.5	-23.9	18.9	1.0
80	76	4-14	15; 14; 42	5.0	- .4	- .9	4.9	206	31.0	-24.3	19.0	2.8
81	78	4-22	15; 34; 30	.7	- .3	- .6	.3	237	23.9	-16.2	17.6	- .9
82	78	4-22	15; 35; 24	1.0	- .1	.3	1.0	238	23.9	-16.3	17.6	- .9
83	78	4-22	15; 35; 48	1.6	- .6	-1.2	.8	238	23.9	-16.3	17.6	- .9
84	78	4-22	15; 37; 00	.6	- .1	.2	.6	238	23.9	-16.3	17.6	- .8
85	78	4-22	15; 45; 06	.5	- .1	- .1	.5	239	24.0	-16.3	17.6	- .7

TABLE 6

Imp-F Current Sheet Parameter Correlation Coefficients, 64 Values

	$\|B_\perp\|$	ΔT	B1	B3	P_x	F_x	T_x	Noise	Sign $B_{\perp z}$	Flip	$B_\perp$	$B_{\perp z}$	TILT	$B3/\Delta T$	Sign $B_{\perp x}$	R	X_{sm}	Y_{sm}	Z_{sm}	$\|Z_{sm}\|$	R_o	$\|R_o\|$	R_c	$\|R_c\|$
$\|B_\perp\|$		-.26	.36	.27	-.04	.33	.18	-.22	.17	.11	.42	.48	.09	.15	.07	-.15	.20	.25	-.05	-.04	-.14	-.01	-.08	.13
ΔT			-.49	-.37	-.30	-.26	-.38	-.16	.13	.17	.17	.12	-.09	-.57	-.16	.19	-.20	-.17	-.07	.20	.17	.17	.13	.09
B1				.79	.21	.07	.20	.38	-.26	.04	-.21	-.15	.43	.87	-.02	-.13	.16	.11	.10	-.23	-.06	-.18	-.02	-.11
B3					.20	-.09	.08	.36	-.12	.00	-.06	-.07	.38	.75	-.09	-.29	.33	.14	-.03	-.16	-.17	-.09	-.14	.04
P_x						.08	.76	.17	-.04	.23	.03	-.04	.17	.22	-.14	-.47	.43	.21	.11	-.01	.06	.08	-.06	.14
F_x							.69	-.16	-.13	-.19	-.25	-.16	-.18	.08	.09	-.18	.10	.13	.04	-.39	-.19	-.33	-.11	-.26
T_x								.01	-.13	.03	-.14	-.13	.01	.21	-.05	-.47	.38	.22	.07	-.28	-.10	-.18	-.14	-.09
Noise									-.18	.16	-.28	-.16	.13	.54	.00	.02	-.07	-.15	.11	-.05	.00	-.03	.05	.10
Sign $B_{\perp z}$										.39	.75	.62	.00	-.39	-.11	-.16	.22	.14	.16	.22	.09	.22	-.04	.29
Flip											.52	.58	-.11	.00	-.38	-.17	.17	.02	.02	.17	.14	.11	-.02	.12
$B_\perp$												.91	.01	-.36	-.18	-.25	.28	.13	-.04	.28	.06	.24	-.05	.31
$B_{\perp z}$													-.19	-.25	-.23	-.16	.20	.08	-.13	.16	.00	.04	-.09	.10
TILT														.25	.26	-.21	.18	.05	.19	.02	.05	.12	.11	.11
$B3/\Delta T$															.01	-.05	.02	-.07	.02	-.32	-.20	-.26	-.12	-.24
Sign $B_{\perp x}$																.14	-.15	.08	.23	.10	.10	.23	.18	.18
R																	-.95	-.55	.02	.30	.20	.27	.32	.05
X_{sm}																		.71	.12	-.26	-.14	-.21	-.24	.07
Y_{sm}																			.59	-.13	.05	-.01	-.02	.31
Z_{sm}																				.08	.37	.33	.38	.44
$\|Z_{sm}\|$																					.73	.76	.63	.61
R_o																						.55	.89	.44
$\|R_o\|$																							.47	.92
R_c																								.36

__Definitions for Table 2__

$|B_\perp|$ — The minimum magnetic field strength at each crossing

ΔT — The current sheet crossing time

B1 — The largest magnetic field strength within one minute of the crossing

B3 — The largest magnetic field strength within three minutes of the crossing

Px — The number of partial crossings per minute

Fx — The number of full crossings per minute

Tx — The total number of crossings per minute (Fx + Px)

Noise — A subjective measure of the deviation of the magnetic field from a straight-line fit to the individual component data at each crossing

Sign $B_{\perp z}$ — The sign of the B_z component at the crossing (+1, 0, or -1)

Flip — The product of Sign B_z on two adjacent (multiple) crossings

$B_\perp$ — The product of $|B_\perp|$ and Sign B_z

$B_{\perp z}$ — The solar magnetospheric z-component at the time of minimum field

TILT — A measure of the inclinitation of $B_\perp$ from the solar magnetospheric z-direction $= \left\{ (B_x^2 + B_y^2)^{1/2} / B_z \right\}\big|_{3min}$

$B3/\Delta T$ — B3 divided by ΔT

Sign $B_{\perp x}$ — The sign of the B_x component at the crossing (+1, 0, or -1)

R — Radial distance in R_e of the satellite at the crossing

X_{sm} — Satellite position at the crossing, solar magnetospheric X-component

Y_{sm} — Satellite position at the crossing, solar magnetospheric Y-component

Z_{sm} — Satellite position at the crossing, solar magnetospheric Z-component

$|Z_{sm}|$ — Satellite position at the crossing, absolute value of Z_{sm}

R_o — The hinging distance of the tail current sheet, $R_o = \dfrac{Z_{sm}}{\sin X_{ss}}$, where X_{ss} is the geomagnetic latitude of the sub-solar point

$|R_o|$ — The absolute value of R_o

R_c — The Russel-Brody circular hinging distance, $R_c = \left\{ Y_{sm}^2 + Z_{sm}^2/\sin^2 X_{ss} \right\}^{1/2}$

$|R_c|$ — The absolute value of R_c
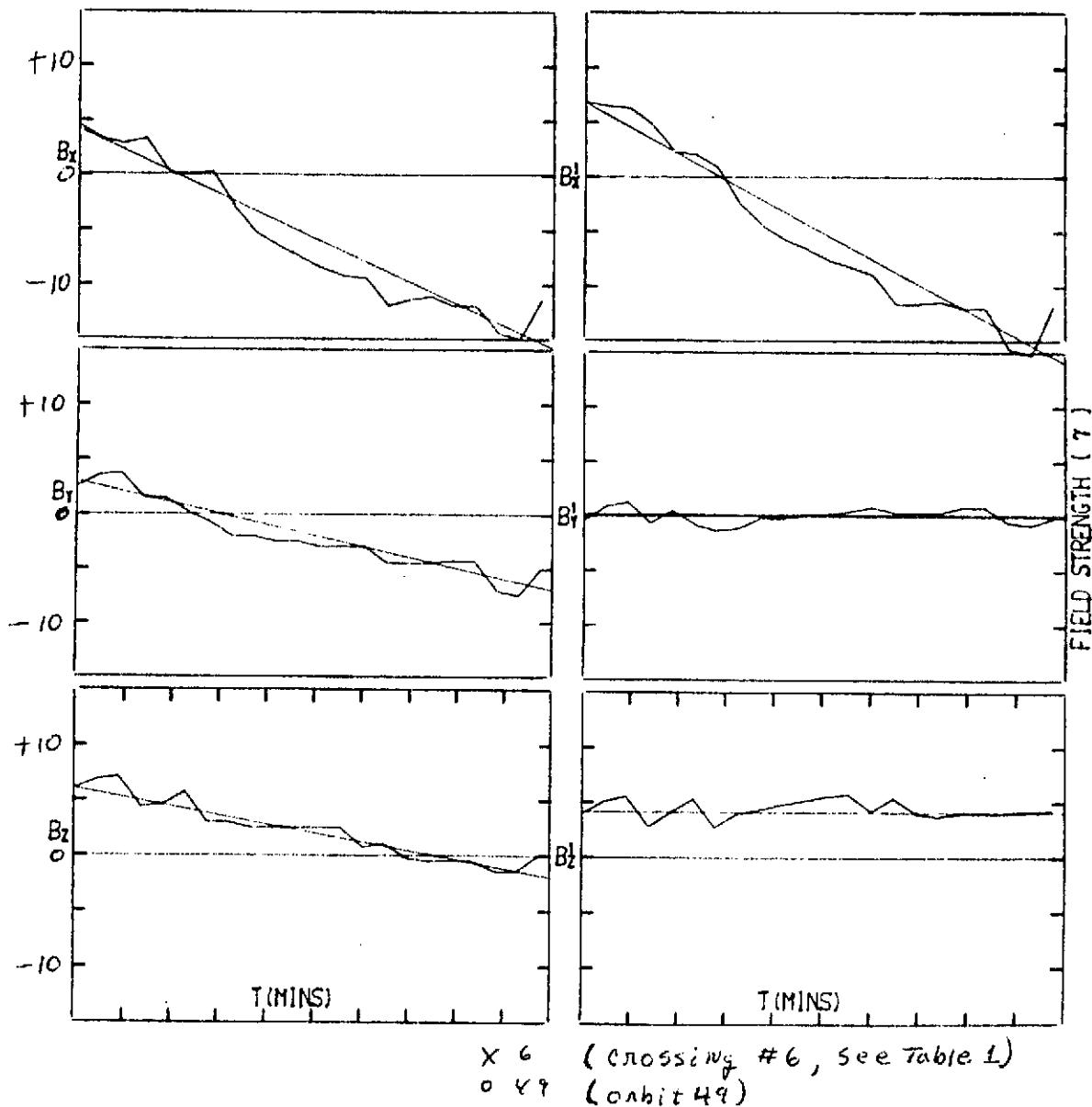
FIGURE 1
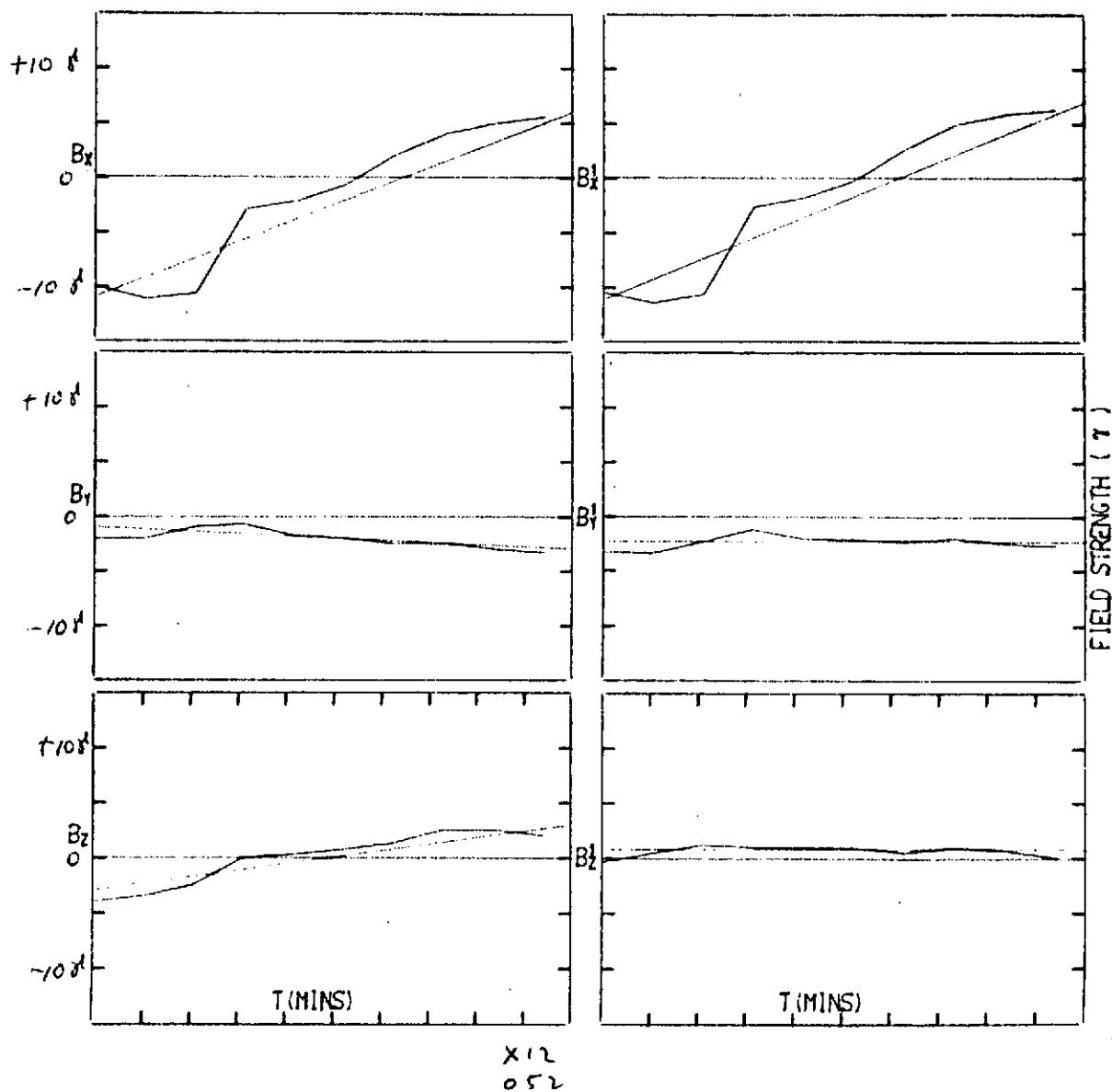
F I G U R E   2
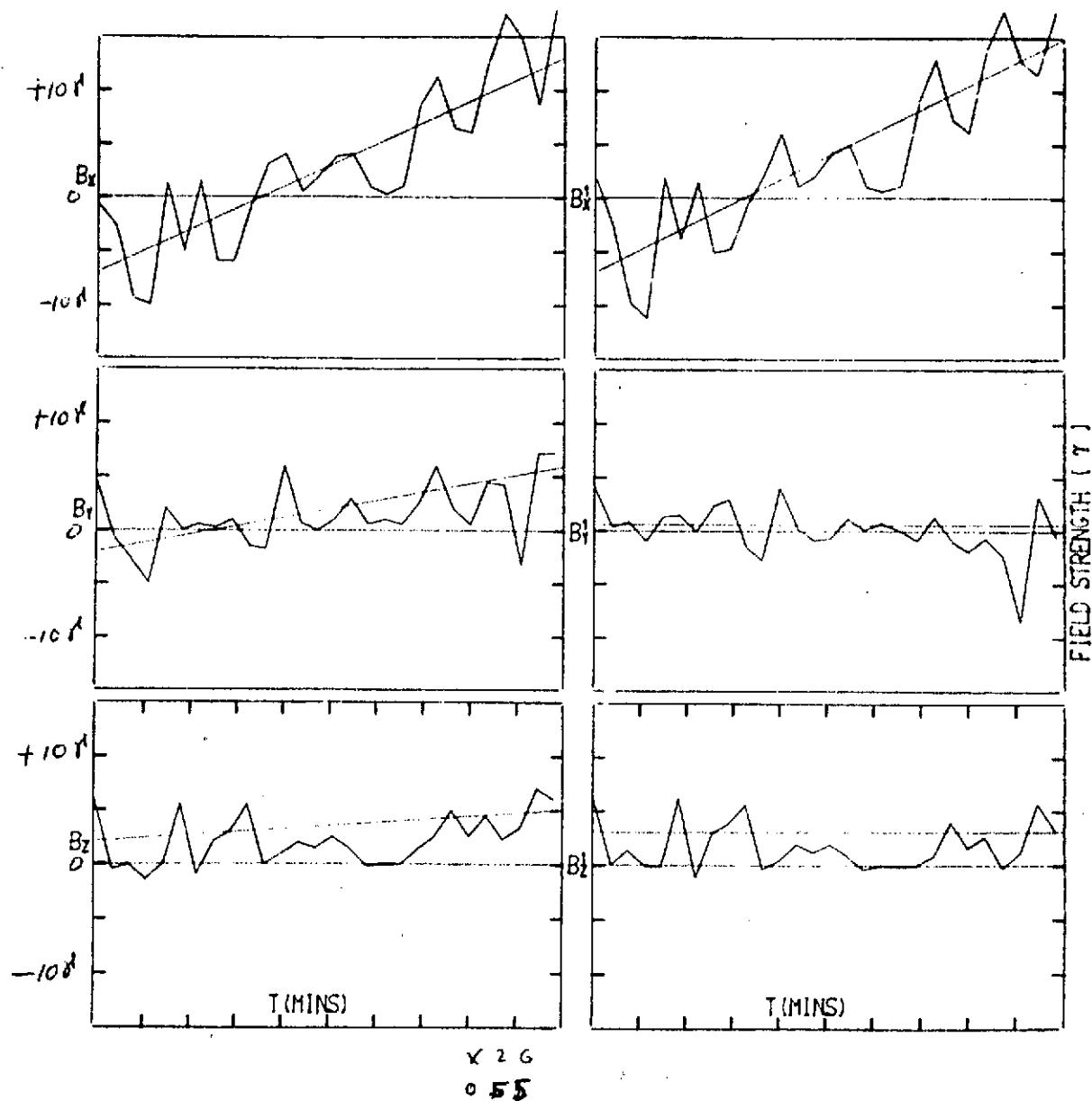
F I G U R E   3
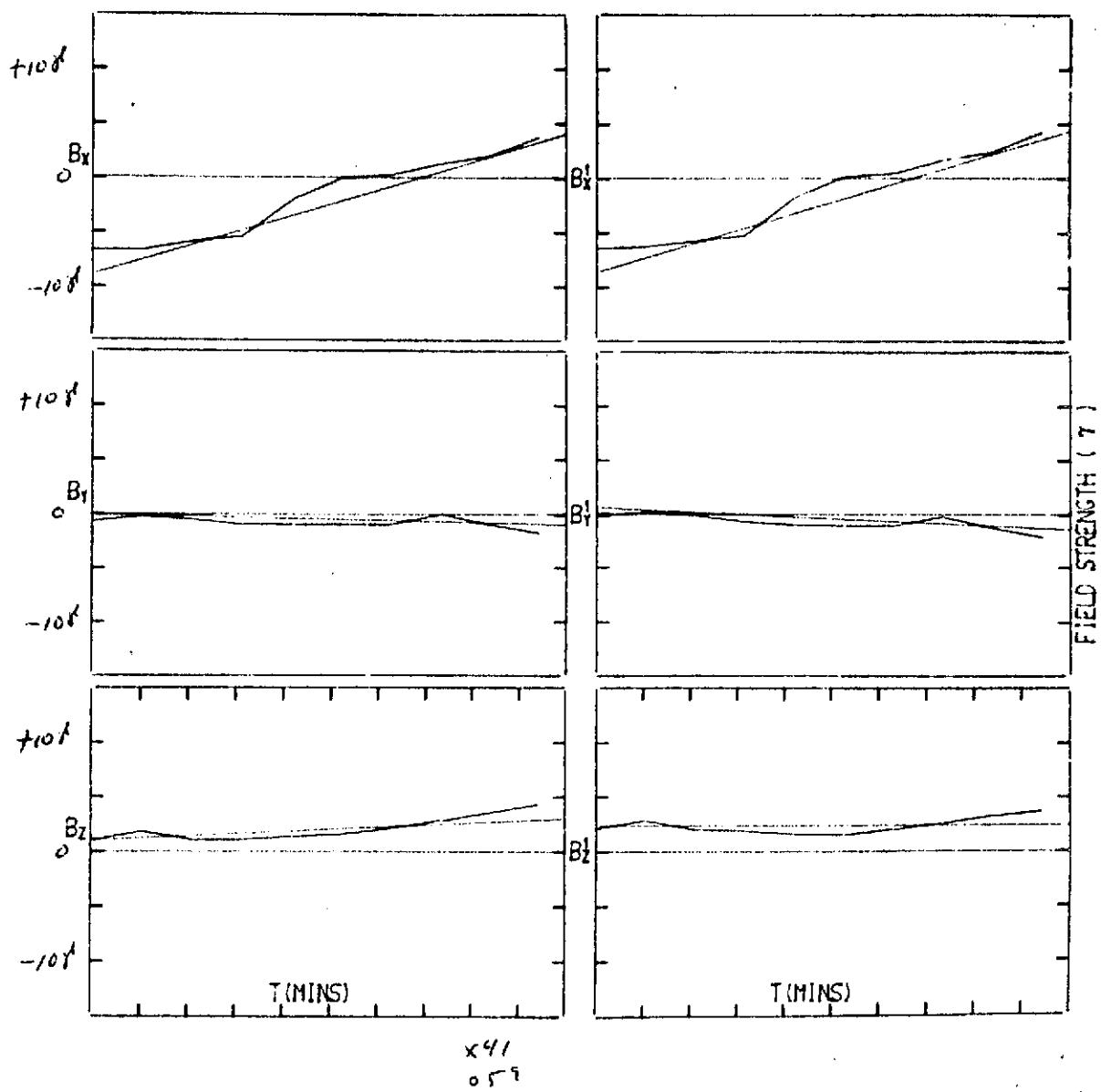
F I G U R E   4
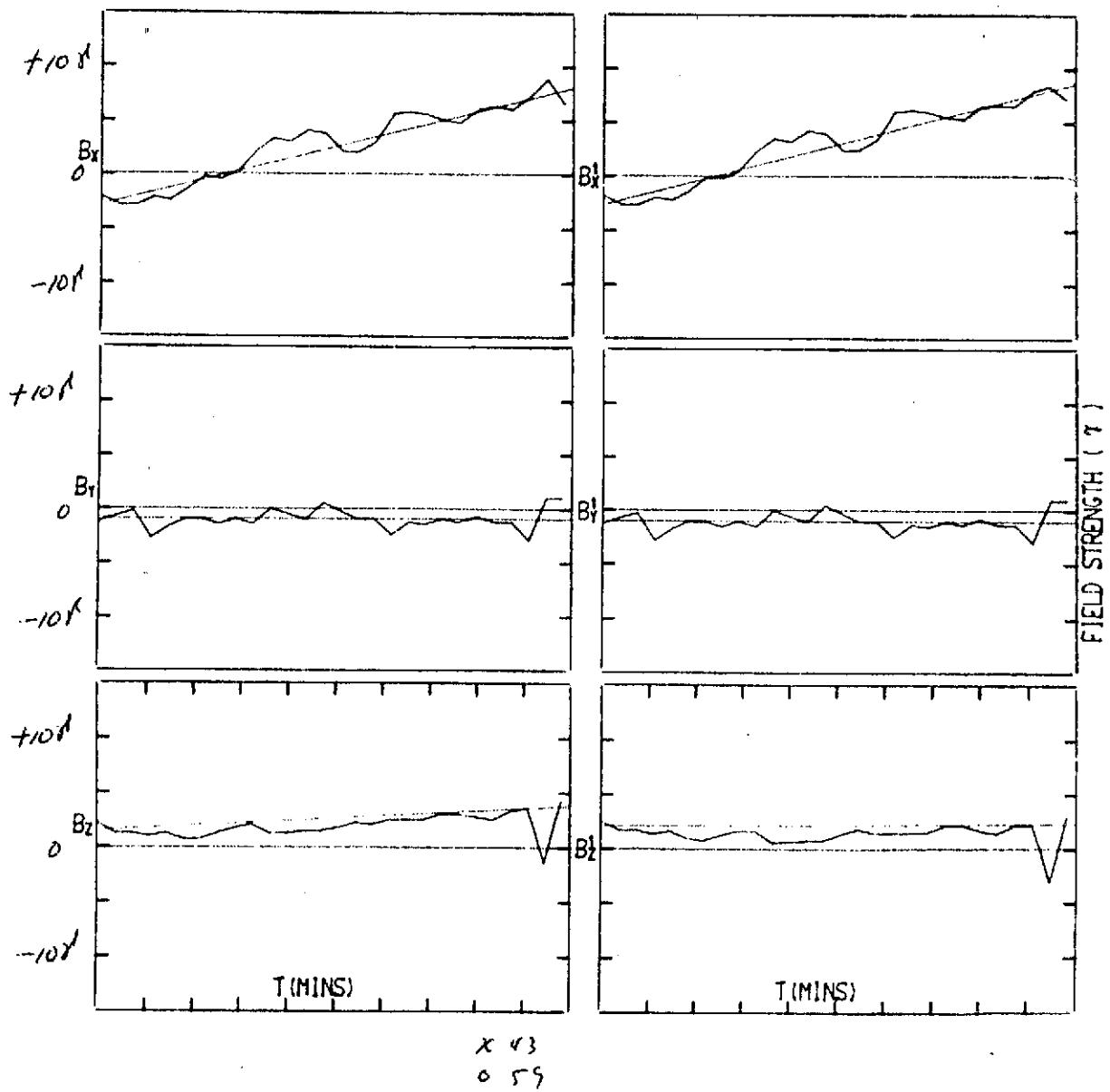
F I G U R E   5
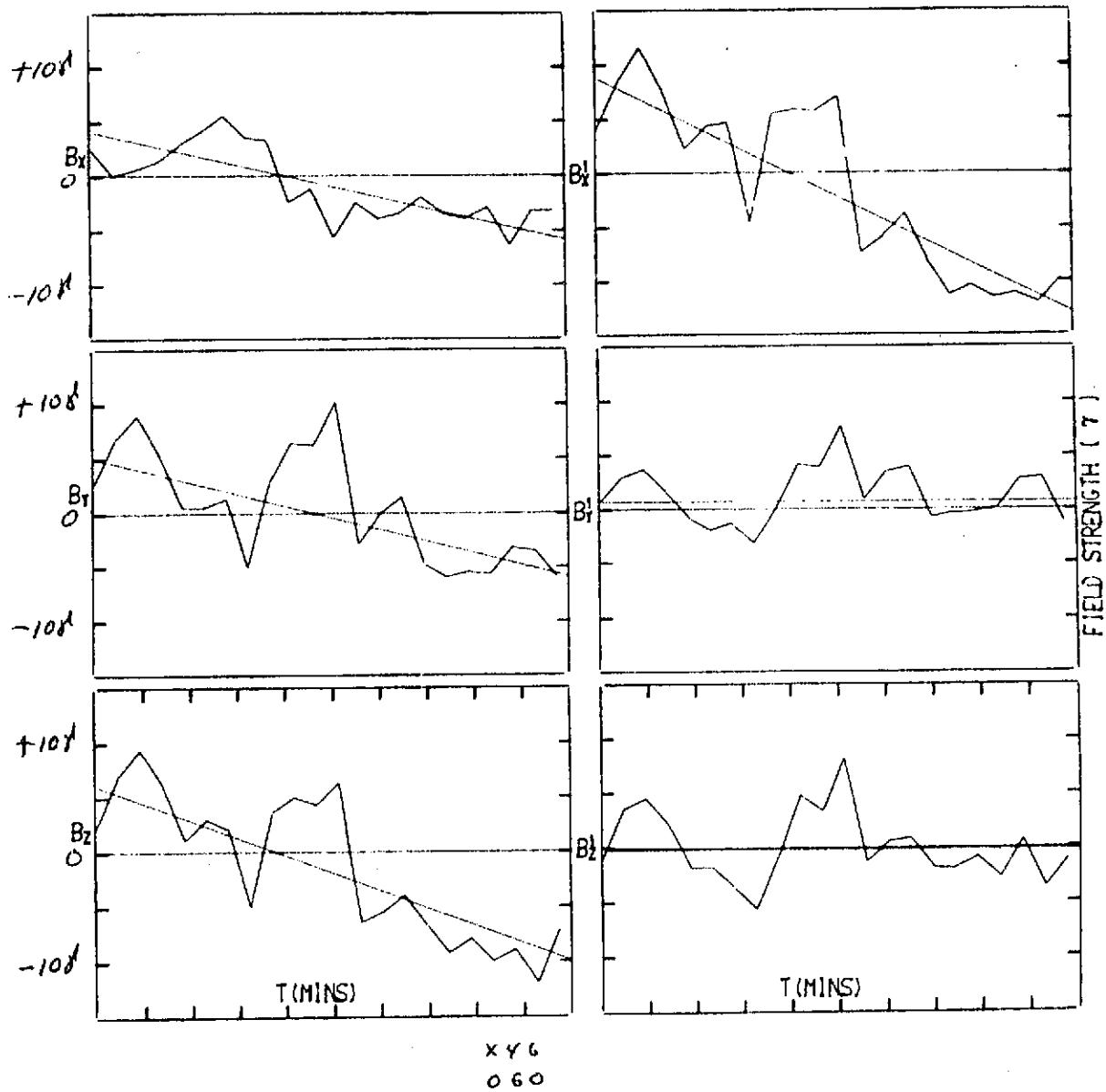
FIGURE   6
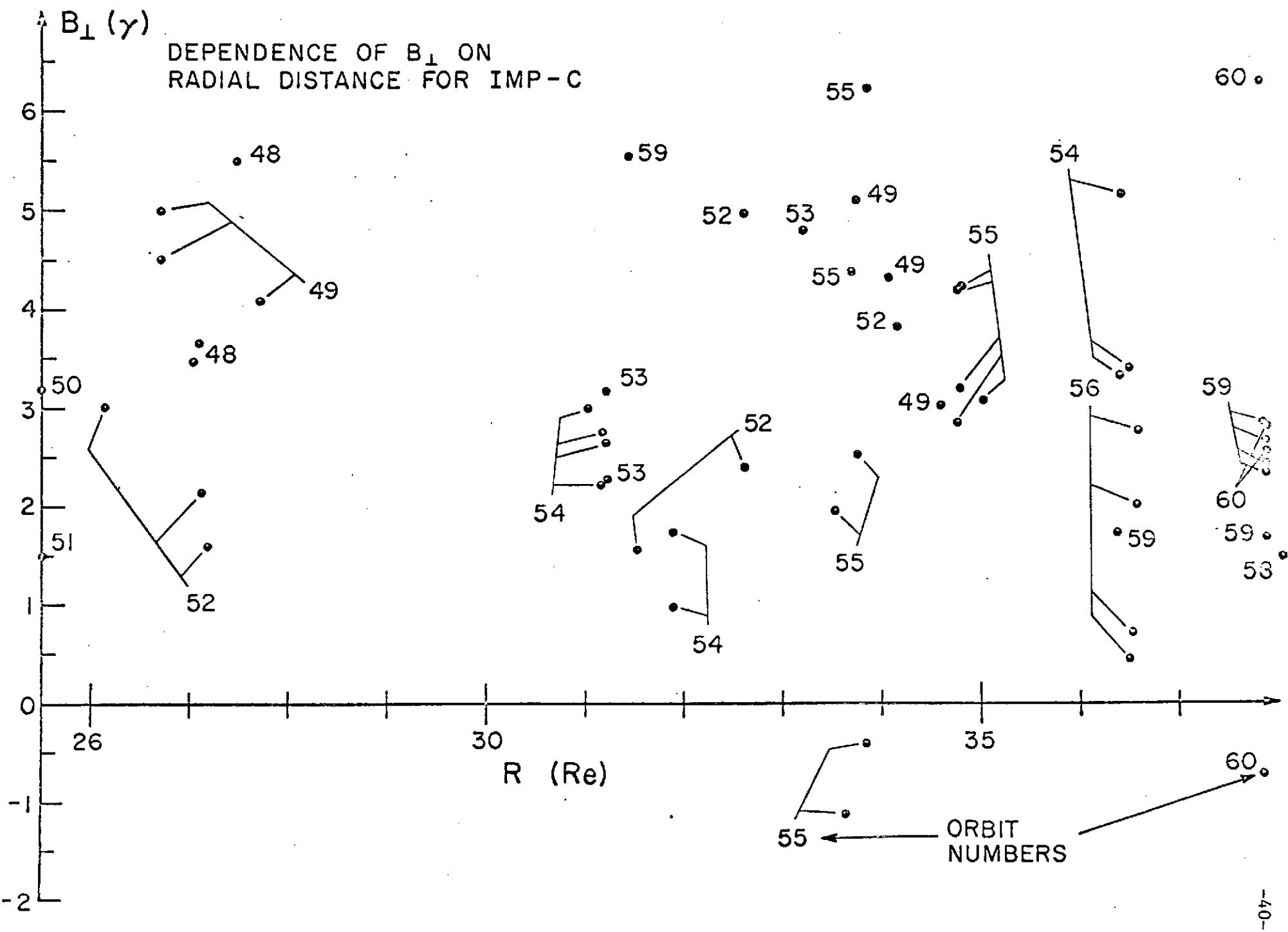
FIGURE 7

F I G U R E   8

DEPENDENCE OF $B_\perp + \hat{s}\cdot\hat{n}$ ON RADIAL DISTANCE FOR IMP-C

FIGURE 9

DEPENDENCE OF $B_\perp - \hat{s}\cdot\hat{n}$ ON
RADIAL DISTANCE FOR IMP-C

ORBIT NUMBERS
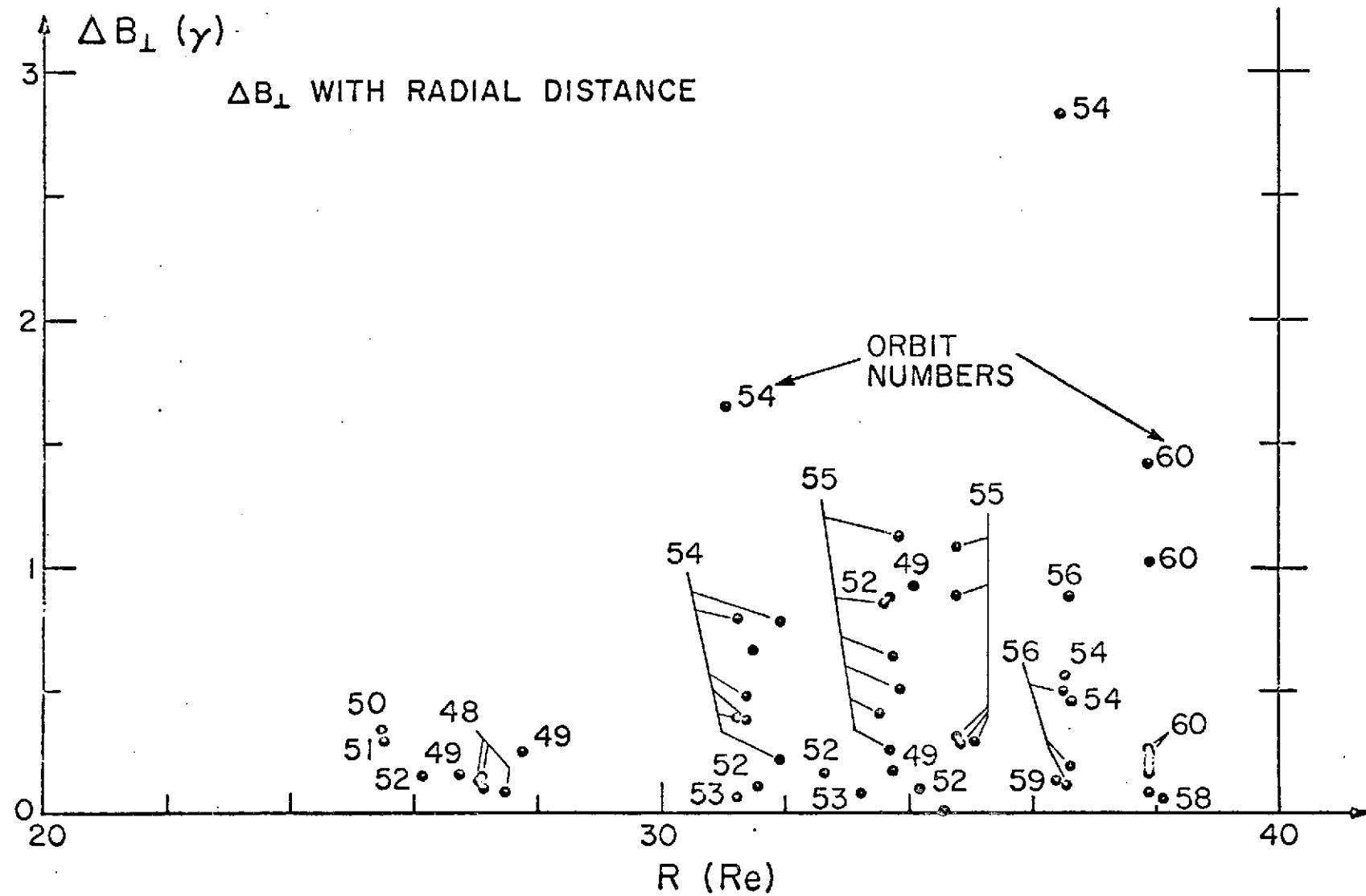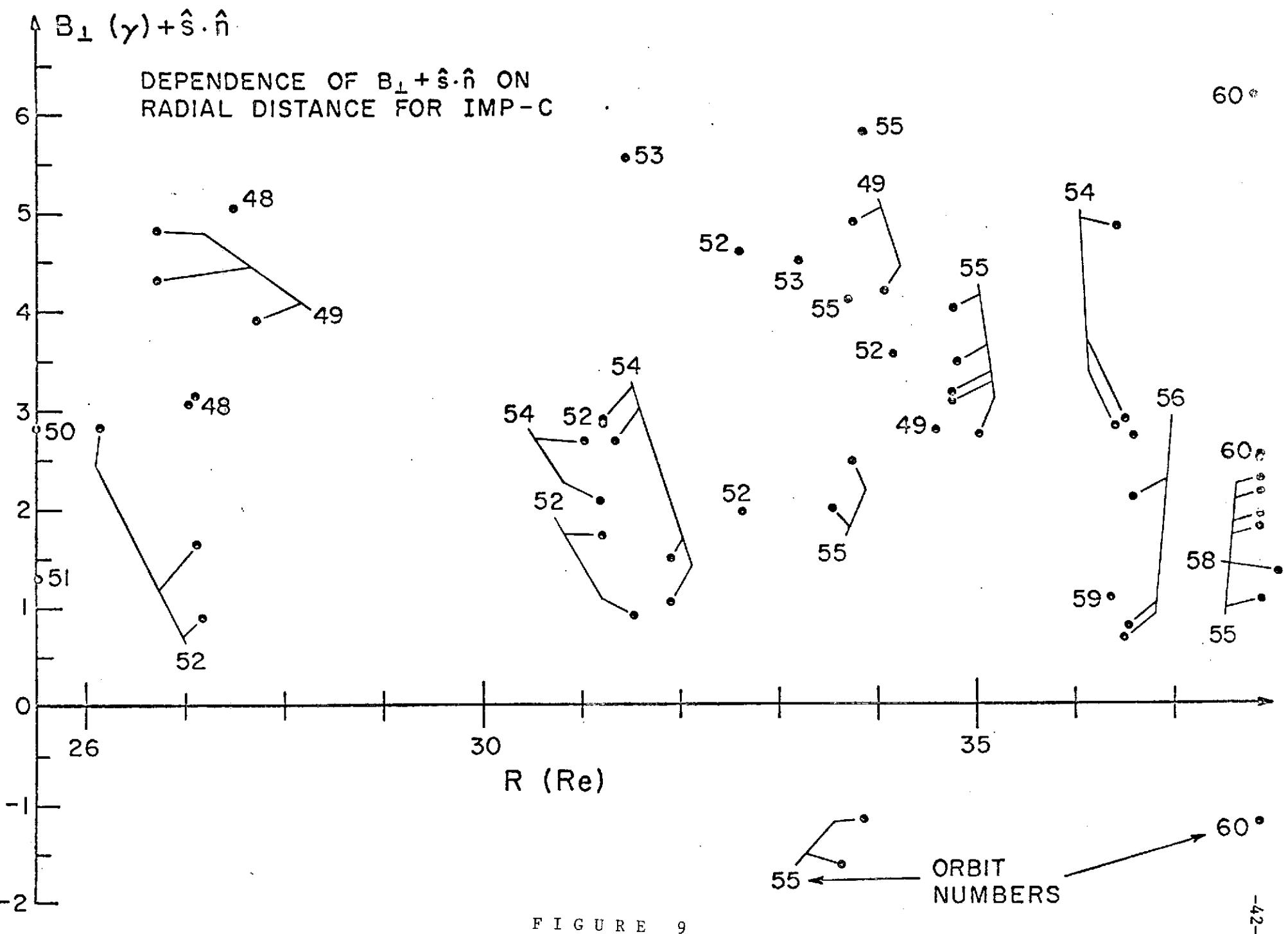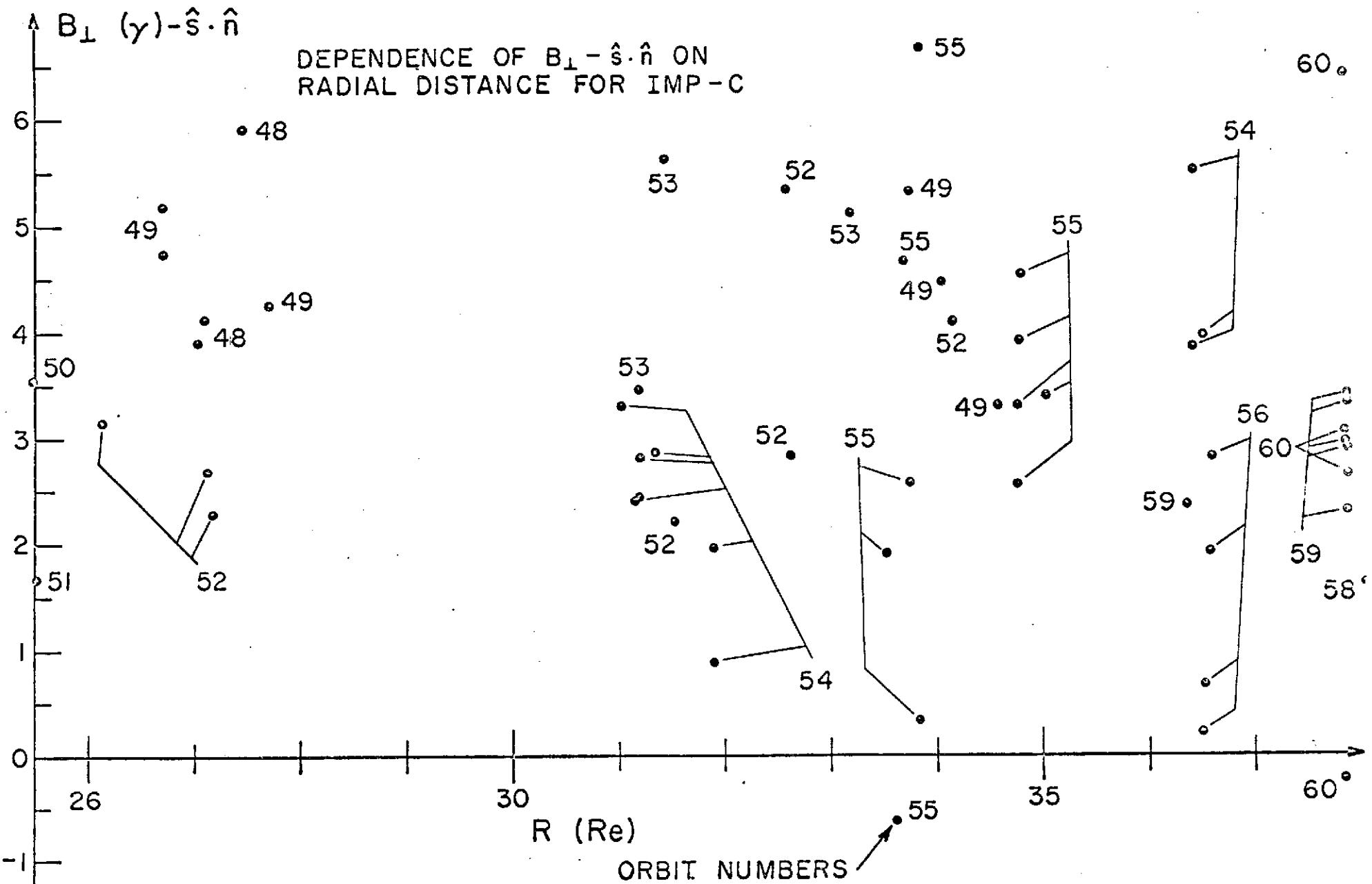
F I G U R E   10
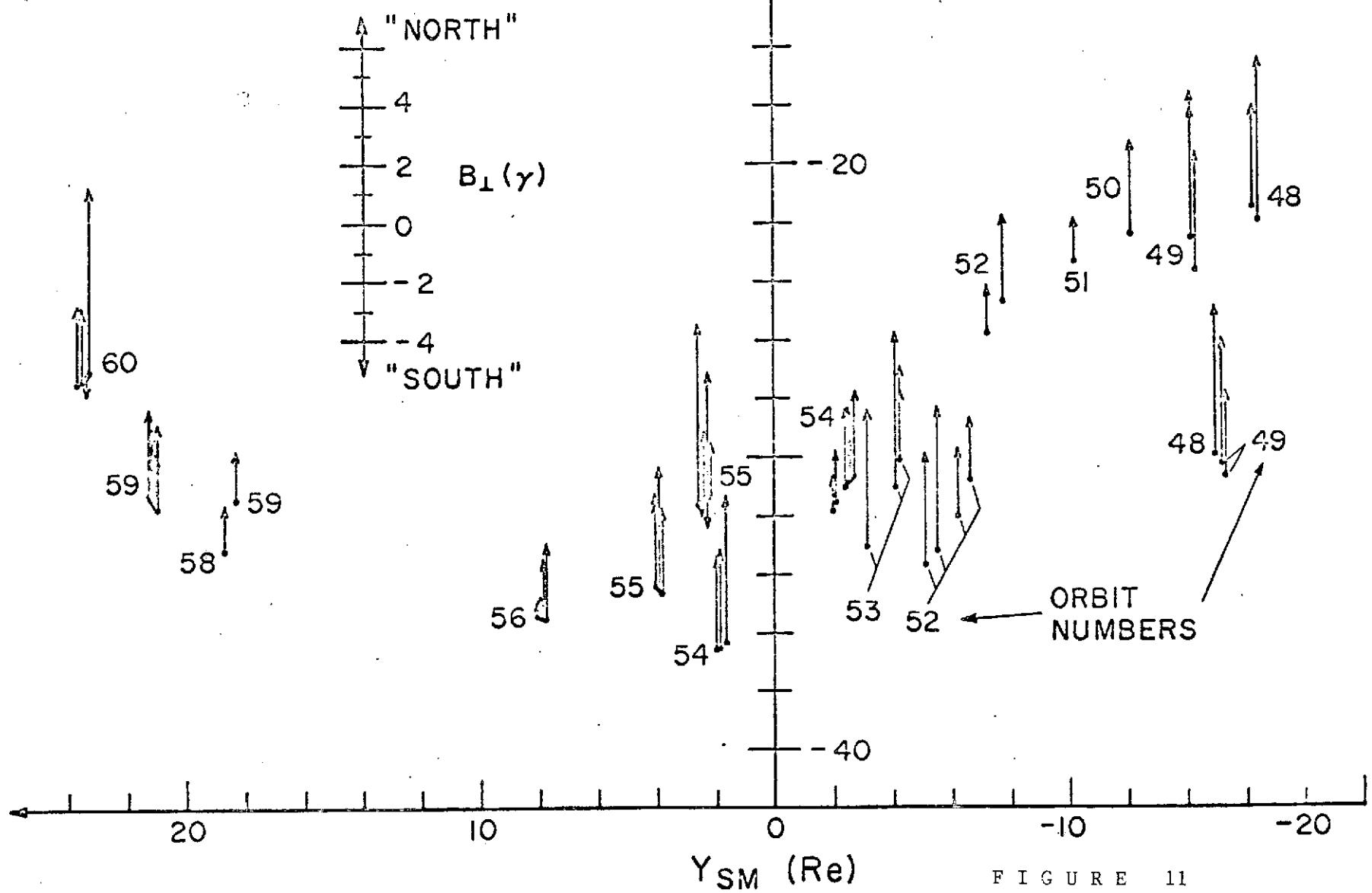
FIGURE 11

δ AT X-Y (SM) POSITION OF
THE IMP-C SATELLITE
(TAN δ = $B_{X\perp}/B_{Z\perp}$)

δ

90° (CCW) ←——→ -90° (CW)

X_{SM} (Re)

−10

−20

51 50 49 48

52

60

59 59

58

55 54

56 53 52 ← ORBIT NUMBERS

49

55 54

−40

20 10 0 −10 −20

Y_{SM} (Re)
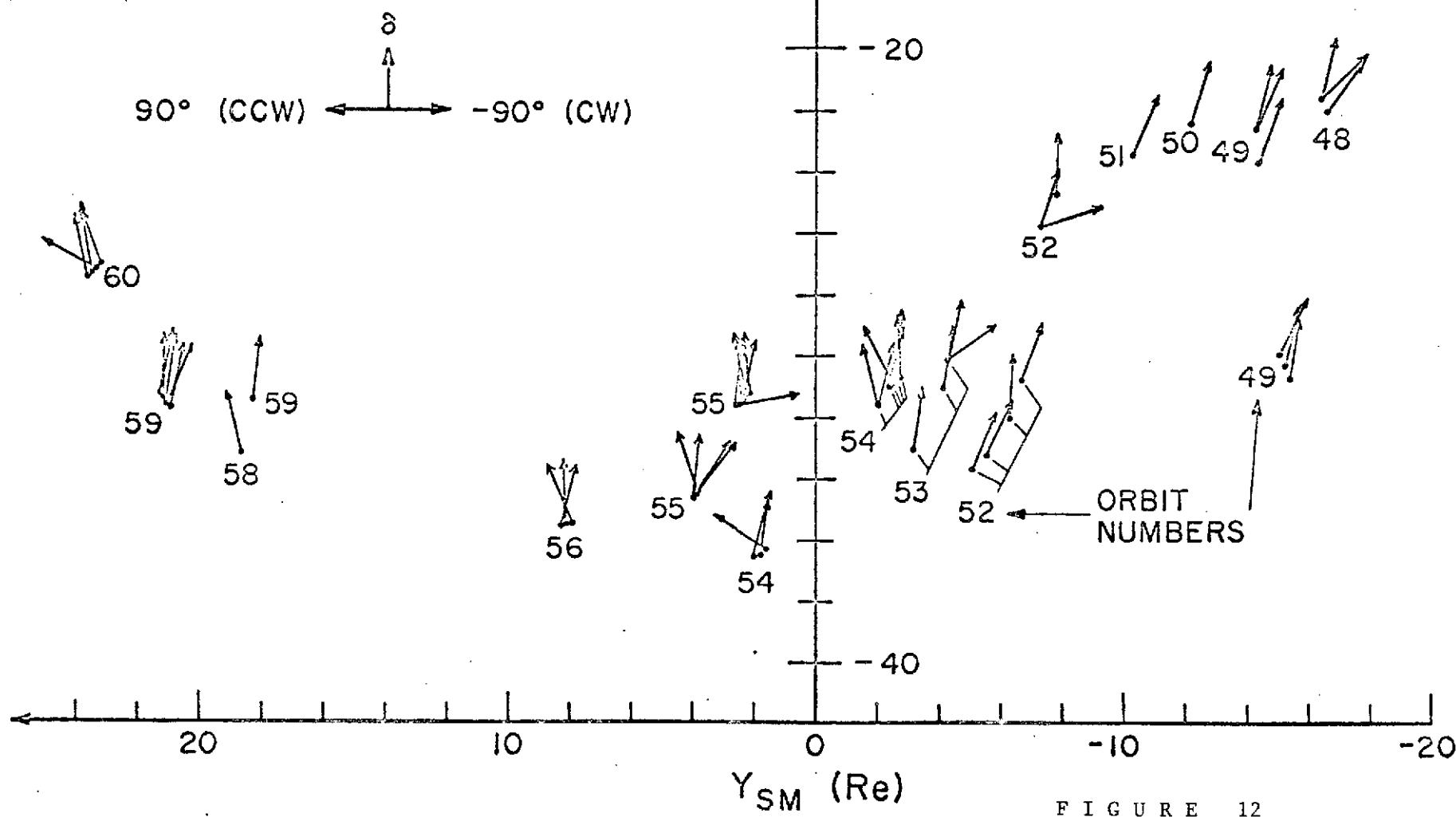
F I G U R E   12

CURRENT PER UNIT LENGTH IN THE (/) SYSTEM AT THE X-Y (SM) POSITION OF IMP-C

$J \times .01$ AMPERES/METER

ORBIT NUMBERS

X_{SM} (Re)

Y_{SM} (Re)

FIGURE 13

Bz NEAR MIN B

ORBIT NO.
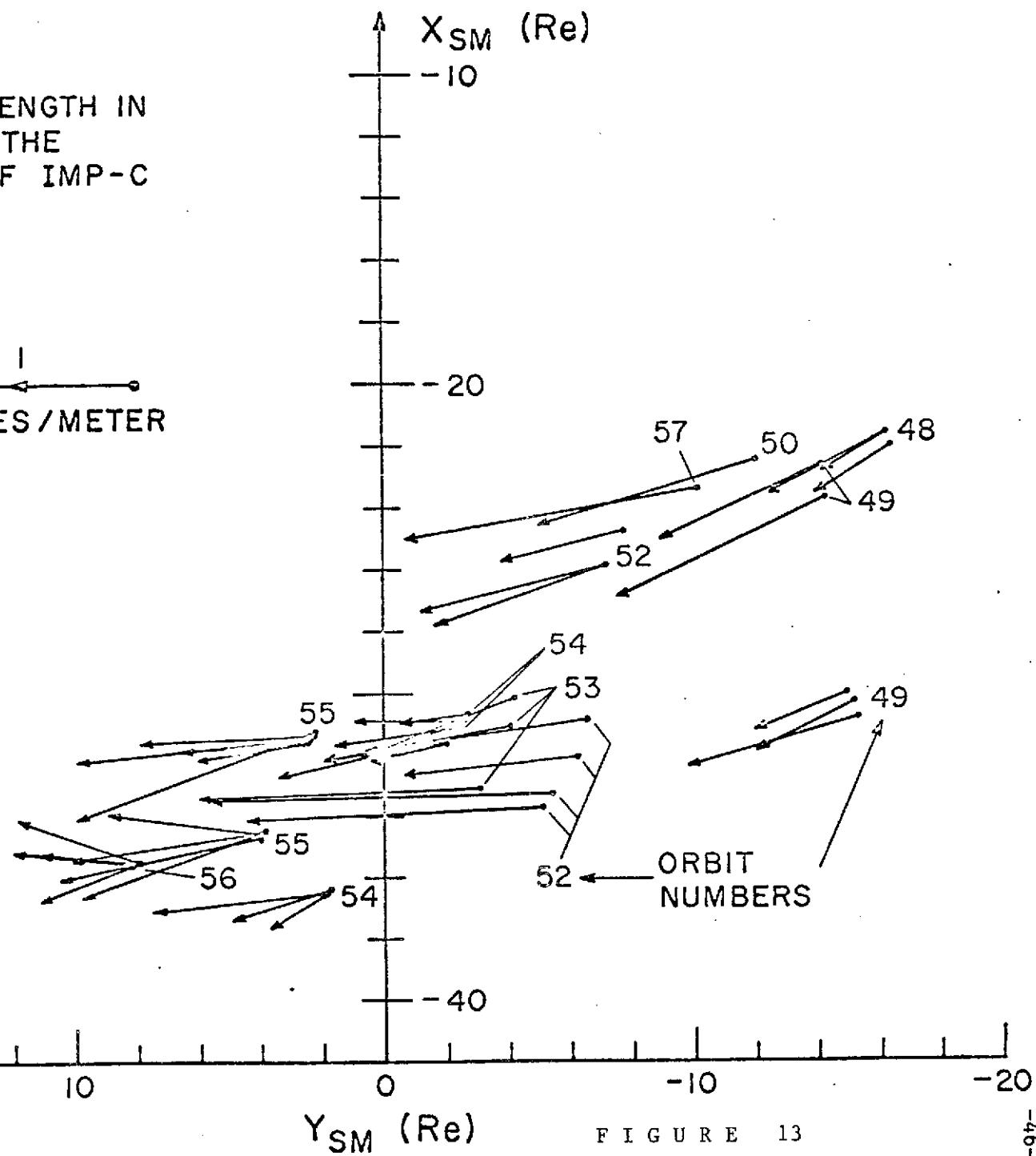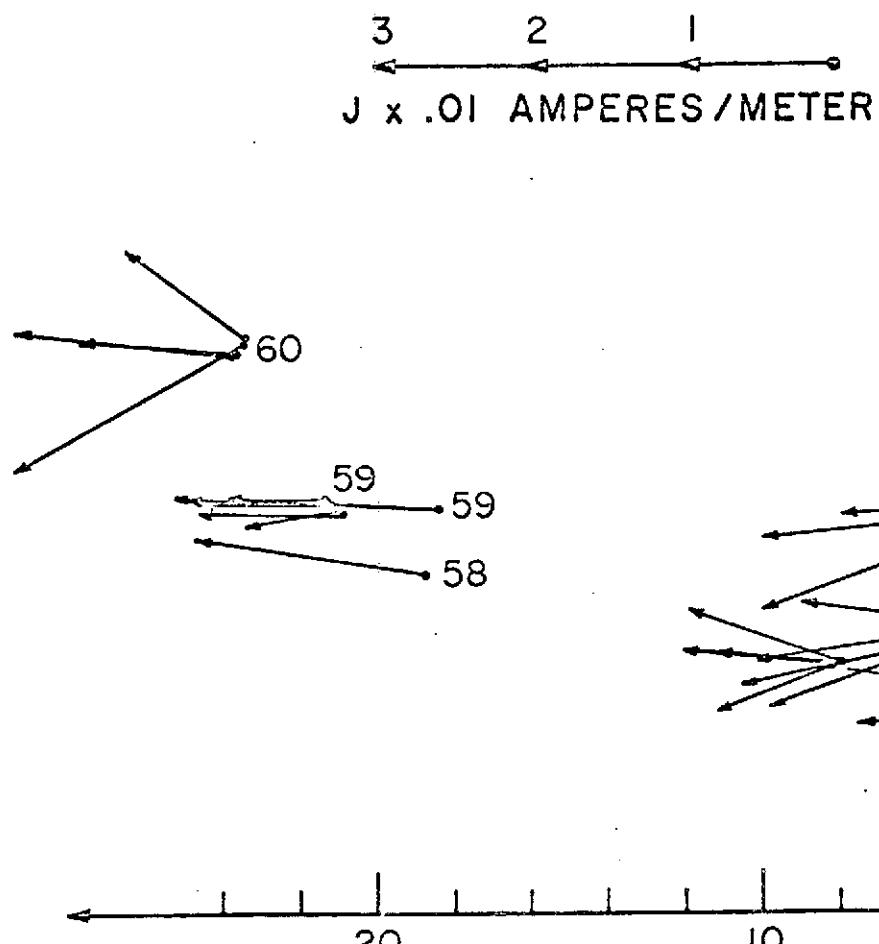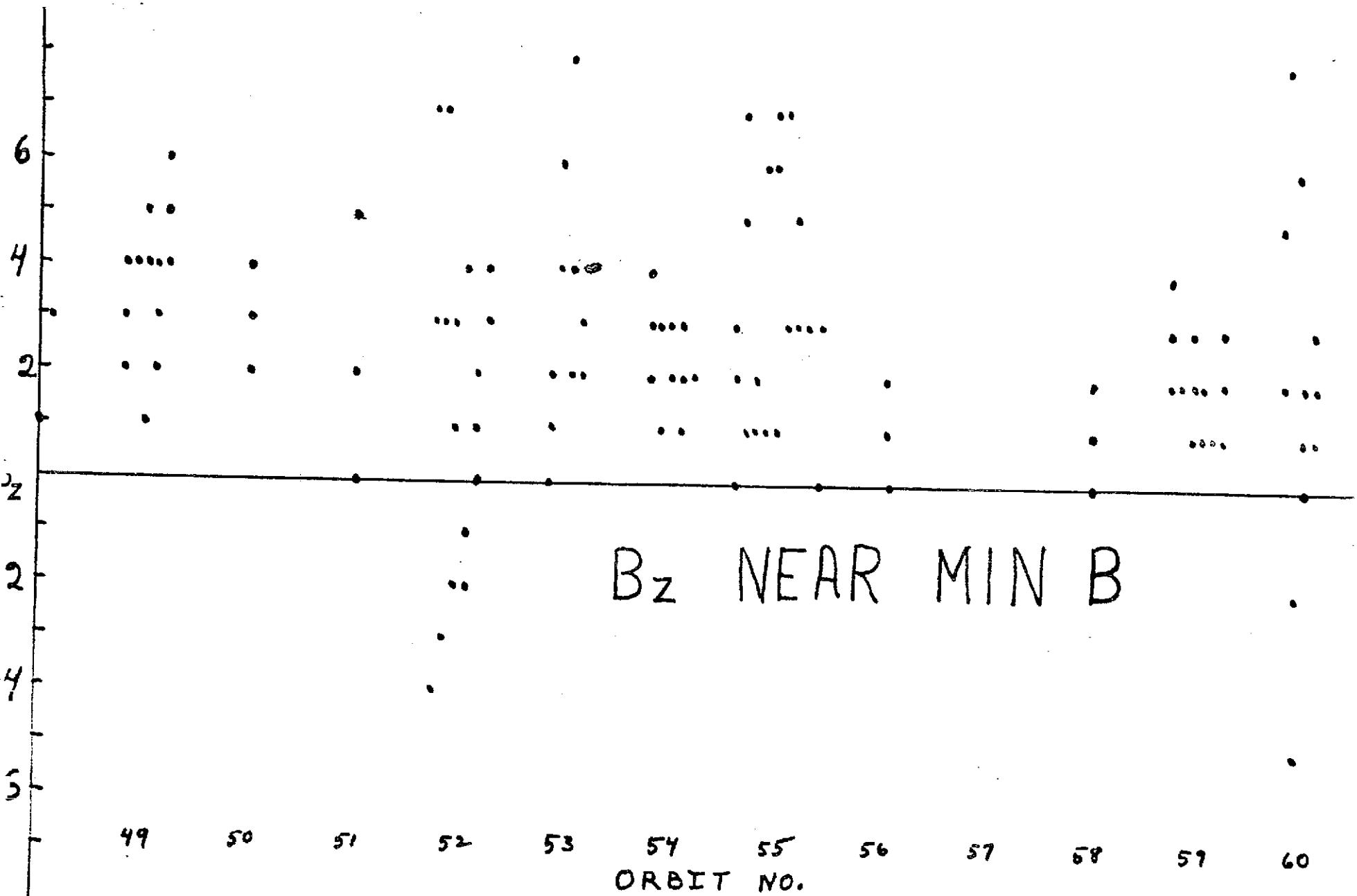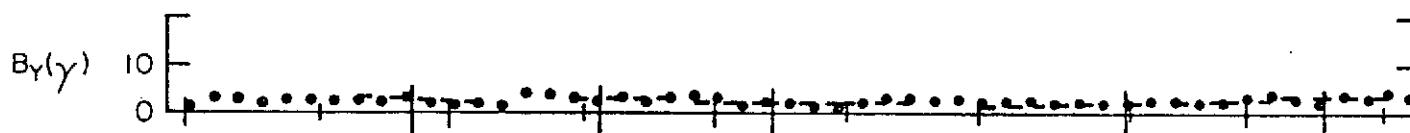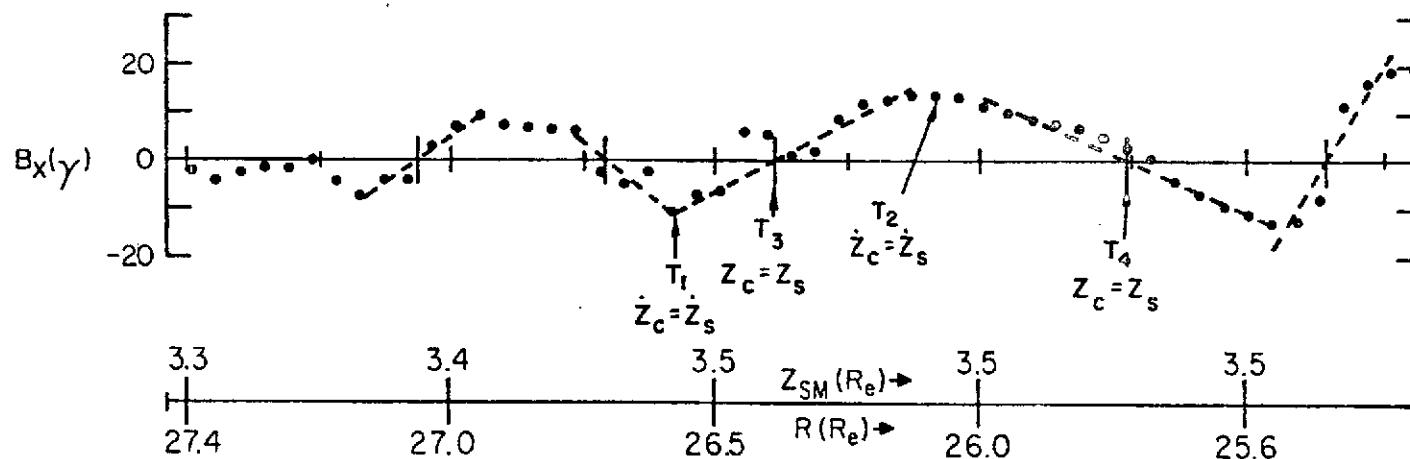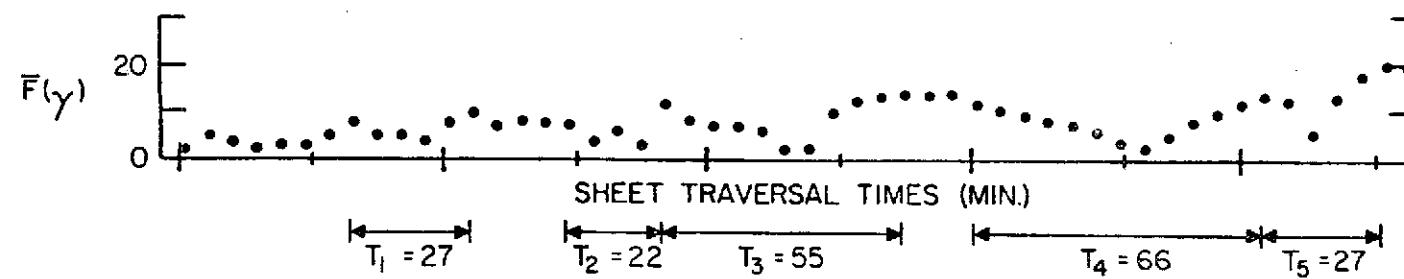
FIGURE 14

IMP-I ORBIT 45
SOLAR MAGNETOSPHERIC
COMPONENTS

FIG 15
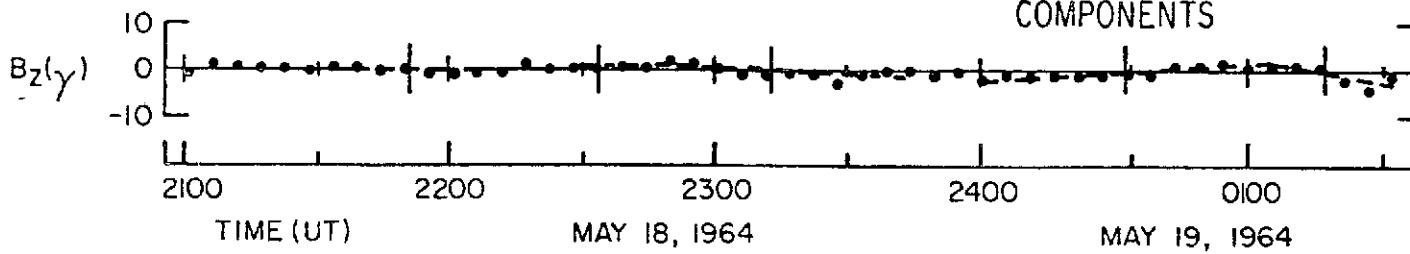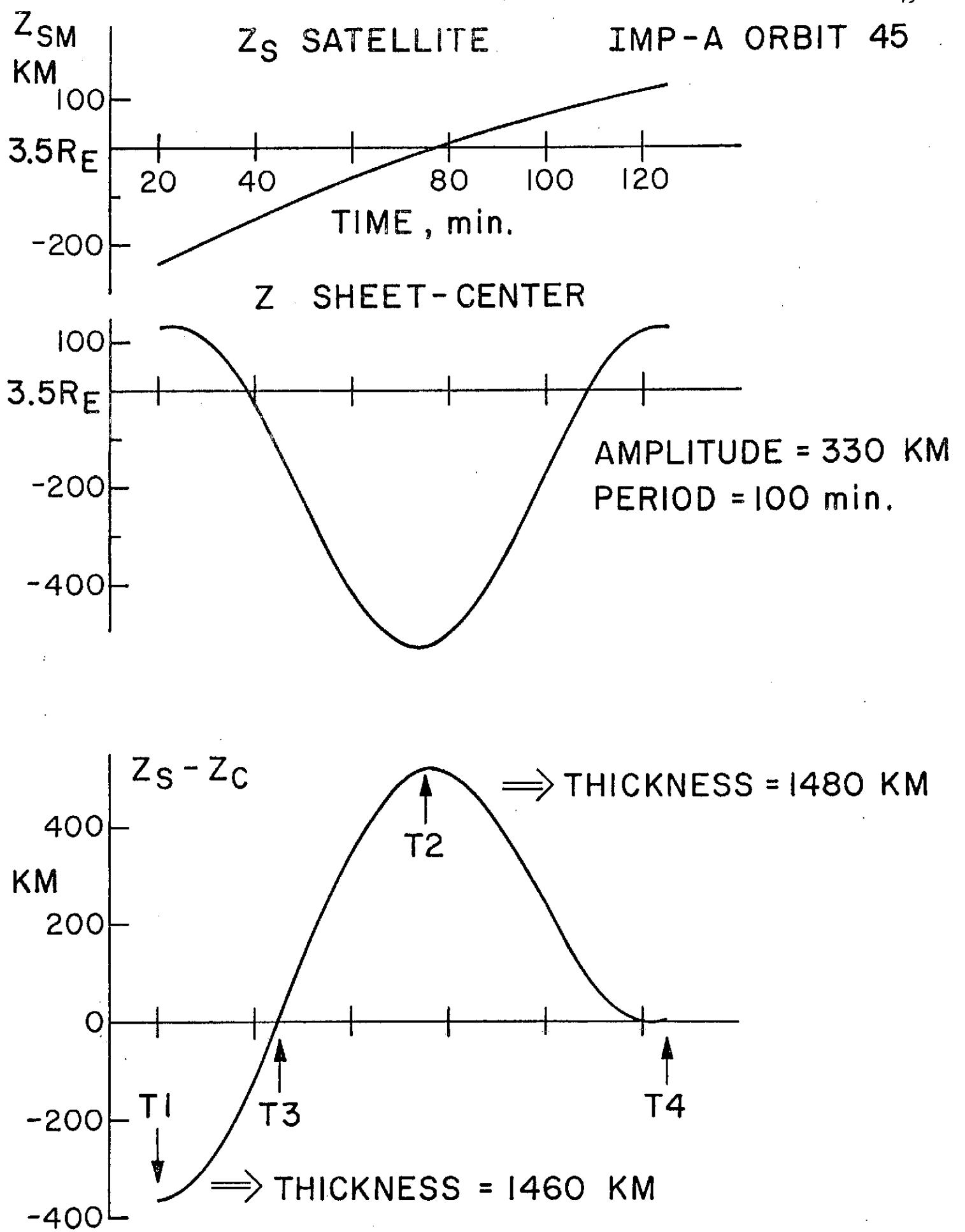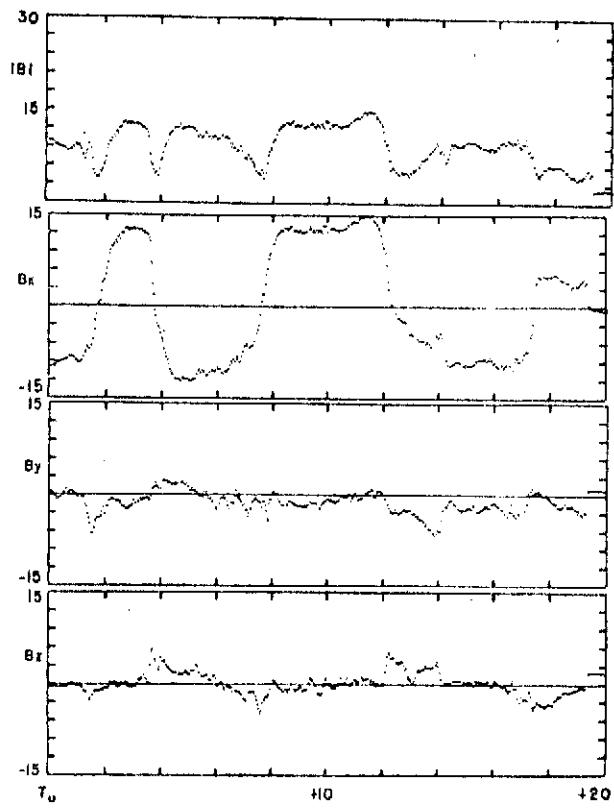
FIGURE 15

F I G U R E   1 6

Imp-F magnetic field data, orbit 72, March 28, 1968, $T_0 = 11:18:30$ UT, division marks every 2 min; solar magnetospheric magnetic field components, division marks every 3 gamma; satellite position (SM): $x = 30.3$; $y = 11.6$; $z = 0.0$ R_N.

F I G U R E   1 7

IMP-F TAIL PARAMETER CORRELATIONS WITH Ae

FIGURE 18

FIG 18

IMP-F TAIL PARAMETER CORRELATIONS WITH Ae

FIGURE 19